Final response to referee #3 comments on paper amt-2020-394

First of all, we would like to thank anonymous reviewer #3 for the very helpful and constructive comments, which served to improve the manuscript. We hope that after addressing all comments the manuscript is easier to understand and the characteristic of the instrument and the viewing geometry, as well as the results are clearer and better explained.

The comments are in bold letters and the answers in normal format. The page and line indicated in the answers correspond to the new version of the manuscript. At the end of the comments the revised manuscript is attached, with the additions in blue and the deletions in red.

Anonymous referee #3

Major comments

My main concern with the paper is that while I'm familiar with many remote sensing and in-situ detection techniques, and with the cloud climatologies they enabled, I had trouble interpreting the results presented in this paper and putting them in perspective against other retrievals. I can't believe I will be the only one. In the minor comments below I try to explain where I had the most trouble understanding.

I am also concerned about the uncertainty in the horizontal location of retrieved clouds associated with the retrieval technique, and I would like to see it discussed, especially when relating the altitudes of detected clouds with tropopause.

The long line of sight of the limb viewing instruments is at the same time its advantage and weak point. An advantage because, as the signal is integrated along a long path, it is sensitive to optically thin clouds, which might be invisible to other instruments. However, this means losing information about the exact position of the clouds. In the following, we try to address all comments to highlight the usefulness of this technique concerning optically thin clouds and try to clarify all doubts.

Minor comments

1. p.1, L. 15-17: "It is possible... veils" this is generic information, which has no bearing on the following discussion and actually creates confusion, as the reader might believe it needs to retain the difference between cirrus, cirrocumulus and cirrostratus to understand what follows. I think it can be omitted.

The indicated lines are omitted in the new manuscript.

2. P.2, L.2: "its" => "their"

Modified (now page 2, line 1)

3. P.2, L.2: I don't understand what are the "typical operational weather satellites" that are equipped with nadir sounders? Please be more specific. To my knowledge "typical operational weather satellites" are geostationary and provide visible/infrared imagery with near-global coverage. "Nadir sounders" make me think of active sensors, such as radars and lidars, which are not found aboard typical operational weather satellites.
The sentence has been changed to: "which complicates its detection by active as well as passive nadir sounders." (Page 2, line 1).

4. P.2, L.15: "Cloud and Aerosol Lidar" – this is not the meaning of the CALIOP acronym. Please fix.
Modified to Cloud-Aerosol Lidar with Ortogonal Polarization (now page 2, line 13)

5. P.2, L.15: "as Dessler (2009)" why mention this?
We mention Dessler (2009) because we want to emphasize the importance of the definition of the tropopause, as the same data set with different definitions yield different results regarding stratospheric cirrus. Both, Pan and Munchak (2011) and Dessler (2009) use the same data set, but obtain different results.
We have rephrase the sentence, so its meaning is clearer: "While Dessler (2009) indicated the existence of a substantial amount of cirrus clouds above the tropopause Pan & Munchak (2011), using the same CALIOP data, demonstrated that the amount of cirrus clouds above the tropopause strongly depends on the definition of the tropopause. Moreover Pan & Munchak (2011) concluded that there is not enough evidence of clouds above the tropopause in mid-latitudes."(Page 2, line 12-15).

6. P. 2, L.16: "there is not enough evidence of clouds above the tropopause in midlatitudes" not enough evidence for what? Please be aware that more recent papers look at cirrus clouds above tropopause using CALIPSO data: e.g. Dauhut et al. 2019 https://doi.org/10.5194/acp-20-3921-2020
By "enough evidence" we mean that there are studies about the existence of stratospheric cirrus, with focus in mid-latitudes, but the frequency of occurrence varies and there is not a wide agreement. Here we summarize the state-of-knowledge from previous studies. We rephrased to make it clearer (please see answer to comment 5). However, in the introduction we refrain from referring to Dauhut et al. 2019 as their inferred diurnal cycle is to a large extent a measurement artefact due to different sensitivities at day and nighttime, see e.g. Zou et al. (2020).

7. P. 2, L.22: "LIDARs" => "lidars"
Modified (now page 2, line 22)

8. P. 2, L.24: If you are interested in SVC cover derived from CALIPSO, please be aware of Martins et al. 2010 https://doi.org/10.1029/2010JD014519, Reverdy et al. 2012 https://doi.org/10.5194/acp-12-12081-2012, or Wang et al. 2019 https://doi.org/10.1029/2018JD029845
We appreciate the recommendation of these very interesting studies. We have included them in the introduction:

"Martins et al. (2010) analyzed CALIOP measurements over 2.5 years and gave an insight into the global frequency of SVC, being more common in the tropics (30-40%). Reverdy et al. (2012) reported a significant population of SVC in the tropical upper troposphere. However, Davis et al. (2010) found that CALIPSO would be missing about 2/3 of SVCs with $\tau < 0.01$. Due to the long path of the line-of-sight (LOS) through the cirrus, typical of limb instruments, clouds that might be invisible to the nadir viewing instruments, are detectable." (Page 2, line 26-30)

9. P. 2, L.26: Again, which nadir viewing instruments?
We mean nadir viewing instruments in general. Our intention is to emphasize that due to the long line of sight of the limb viewing instruments, optically thin clouds can be measured by limb instruments, but might be invisible to the nadir ones.

10. P. 2, L.33: I understand that this is the resolution of a pixel looked on straight from the plane, i.e. in a plane normal to the direction of view. What is the volume of air described by the measurement in a straight line away from the plane, I.e. along the line of sight? Is the tangent altitude the point of lowest altitude along the line of sight? Please mention these precisions.
Due to the nature of the limb retrieval technique, specifying the volume of air measured by the instrument is a challenging task. The lines of sight along which the measurements are taken, are infinite, therefore, the volume would also be infinite. Even restricting it to the atmosphere is not necessarily sensible as the amount of emitting molecules decreases exponentially with increasing altitude. Practically, we restrict it for this computation to the altitude of the aircraft. The point spread function (PSF) of the instrument also doesn't have a compact support such that the horizontal/vertical extent of the measured cone needs to be defined in some fashion to be finite. The tangent point is defined as the point closest to the earth of the idealized pencil-beam thin line of sight. The PSF of a pixel can be computed astonishingly well from a theoretical Airy disk using the aperture of the instrument of 3.6cm and using here $830 cm^{-1}$ as a reference wavelength. The vertical width would then correspond to 0.032° and horizontally we observe 1.53°. This corresponds to a rectangle of $15 m^2$ area one km away from the aircraft, growing quadratically with distance. For a line of sight pointing to a tangent point (neglecting refraction for simplicity) 3km below the aircraft, the tangent point would be roughly 200km away corresponding to an observed area of roughly 600000 m^2 at this point. As such the volume of air covered by this pyramid between aircraft and tangent point is roughly $40 km^3$. Following it further until it reached again the altitude of the aircraft gives an observed volume of $319 km^3$.

The definition of the tangent altitude being the point of lowest altitude along the line of sight has been added in the caption of Figure 2 (following comment 13) and in the first appearance of the term tangent altitude: '…at a tangent point altitude (i.e. the closest point of the line of sight to the Earth's surface) of 10 km…' (Page 3, line 1).

11. P. 3, L. 9: "step stone" => "stepping stone"?
Changed to: 'stepping stone' (Now page 3, line 16).

12. P. 3, L. 23: "one profile": what is the vertical resolution of one such profile?
The vertical resolution is given by the full width at half maximum of the averaging kernel, which describes the relation between the retrieved quantities and the true atmospheric state.

The following figure illustrates the vertical sampling of one profile for an altitude observer of 14.21 km for all tangent point altitudes. The right plot indicates the altitude of the tangent points and the left plot the corresponding pixel row of the detector. Each pixel has the same point spread function (PSF) described by an Airy disk with an aperture of the instrument of 3.6cm and using 830cm^{-1} as a reference wavelength. The vertical sampling is higher, the closest the tangent point altitude is to the observer altitude, as the projection of the PSF gets wider the further the tangent point is. We have added in the manuscript an example: "The vertical sampling is higher the closest the tangent point altitude is to the observer altitude, as the projection of the PSF gets wider the further the tangent point is. For example, if the observer altitude is 14.7km, at a tangent point of 13km, the vertical sampling is about 88m, at 10km of about 150m and at 8km of about 179m." (Page 4, line 2-3).

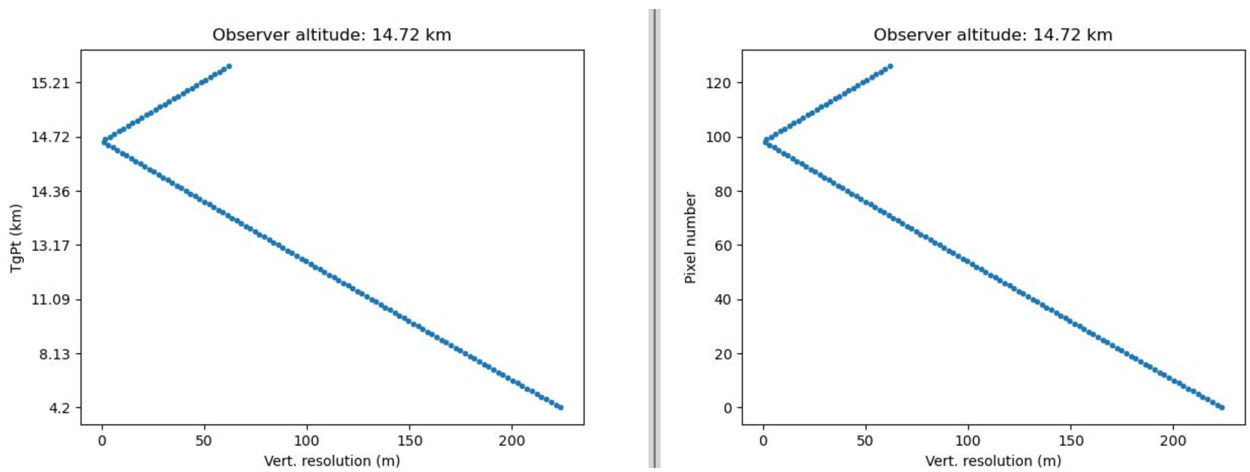

13. P. 6, Figure 2: I'm not overly familiar with measurements like GLORIA's, so please forgive me if I ask obvious questions. Here are a few things I think I've understood, that I don't think are explicitly stated before the figure, and that would help its understanding if they were:

- I understand each blue line in Figure 2 to be a different line of sight.

Correct.

- I understand GLORIA scans successive lines of sight, each corresponding to a different angle with the horizontal, and each describing cloud information along the line of sight that corresponds to that angle and to a minimum altitude level.

Correct.

- I understand that the cloud information (IWC) is integrated along the line of sight, and the obtained IWP used as cloud indicator. It follows that the instrument documents the vertical distribution of clouds across a very large horizontal distance that varies with altitude, eg for 7km ASL the horizontal distance described is 420km, for 15km it is 660km, for 18km it is 720km, etc (according to the lines of Figure 2).

For determine the presence of clouds with GLORIA we do not use IWP. IWP is used only for the ERA5 data, as a way to identify clouds in the ERA5 data set, adapted to the viewing geometry of GLORIA. This way, we are be able to compare the ERA5 data set with the GLORIA results. GLORIA measures radiance and this signal is the one that is integrated along the line of sight.

The cloud index, i.e the ratio of the mean radiances between the spectral region 788.2 – 796.2 cm^{-1} and the spectral region 832.4-834.4 cm^{-1}, already used in other studies, is one of the methods we use to identify clouds. The second method is the extinction coefficient, which is retrieved using the model JURASSIC2 to solve the inverse problem in which the radiance is the input.
Related to the horizontal distance, as you can see in the following figure, the line of sight would go twice through an altitude of 7 km, first at a horizontal distance of 190 km and then of 440 km. 15 km would be at a horizontal distance of about 680 km and 18 km at around 730 km (yellow rectangles). The lowest line of sight is the longest one.

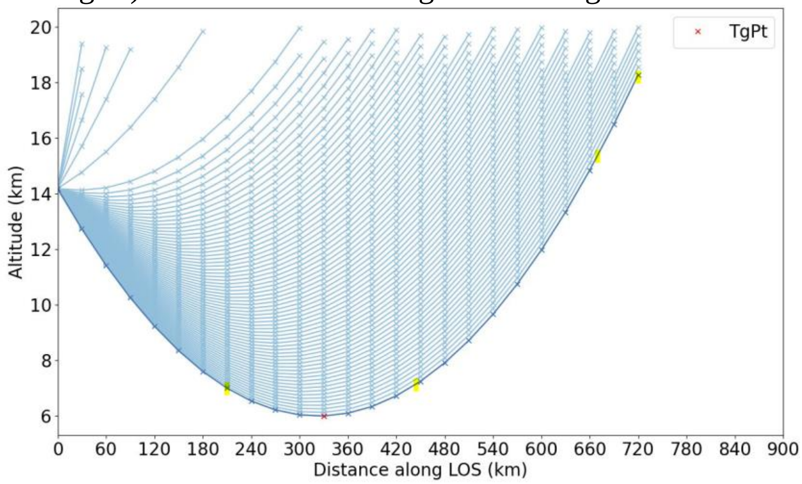

For other line of sight, with a tangent altitude point, e.g., at 12 km, the horizontal distances would change. This line of sight would not go down to 7km, 15 km would be at 450 km and 18 km at 520 km.

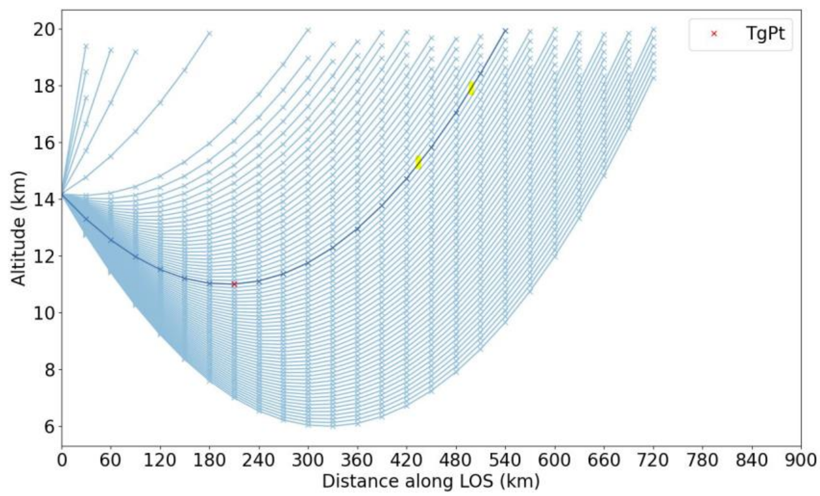

- I understand that analysis of GLORIA data can tell a cloud is located along a given line of sight, which provides some insights into its spatial location. Each value of GLORIA's vertical cloud profiles is representative of a quite long path, that is longest at highest altitudes, and neither horizontal nor vertical: for instance, the lowest line of sight in Figure 2 will document cloud presence at ~12km ASL 60km away from the plane, at

~10km ASL 120km away, down to ~6km ASL 330km away, and then up again. Due to refraction, each line of sight is not a perfect straight line.

The lines of sight should be straight lines, but due to the refraction in the atmosphere, they are slightly curved. When plotted in a reference system with earth surface as a straight line, the lines of sights adopt a parabolic form. The tangent point moves away from the observer with decreasing tangent point altitude and the longest line of sight is the lowest one. Please see the answer to the previous point of this comment.

My understanding of those points sometimes comes from later sections of the text. If my understanding is correct, could you please find a way to include those points in the text before reaching Figure 2, or in the legend of Figure 2, to help readers unfamiliar with the approach?

In order to provide a clearer description of the viewing geometry, we have included the points of this comment in the caption of Figure 2:

"a) Example of the measuring geometry of GLORIA. The tangent altitude point is the closest point of the LOS (line-of-sight) to the surface. b) Example of the measuring geometry of GLORIA in a Cartesian system. Each blue line represents a different LOS that corresponds to a different elevation angle. The LOS is not a perfect straight line due to the refraction in the atmosphere and when plotted in a reference system with the Earth's surface as a straight line, it adopts a parabolic form. Each LOS is associated to a different tangent altitude. The horizontal distance of each LOS can extend several hundreds of kilometers. The lowest LOS are the ones with the largest path. The radiance measured by GLORIA is integrated along each LOS and contains the information related to the presence of clouds. The radiance from all LOS are recorded simultaneously. The red line indicates the tropopause (TP) from ERA5 along the corresponding LOS, in dark blue."

Also Figure 2 has been modified, as we considered the following image can help to better visualize the geometry.

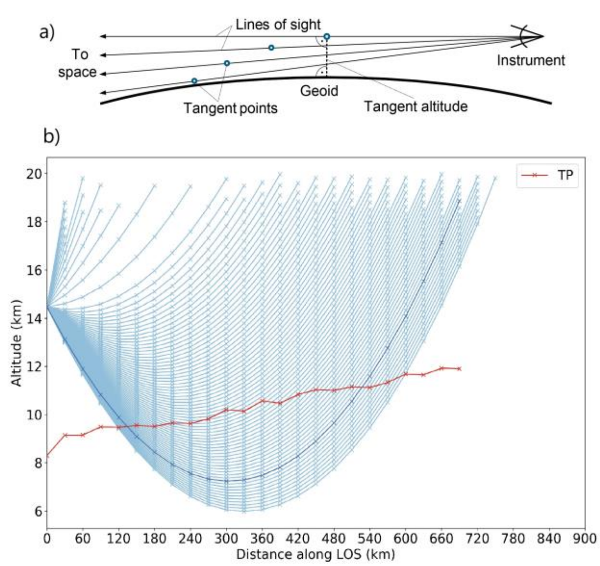

14. Figure 2: Would it be possible to add a cloud to this figure and show next to it the cloud profile that would then be generated, with the final base and top altitudes? It would help interpretation by non-experts.

The aircraft is at ~14 km. If we assume a 1D cloud layer horizontally infinite, which could be a representation of a large scale cirrus field, indicated by the thick blue line, the CTH would be referenced at 11 km.

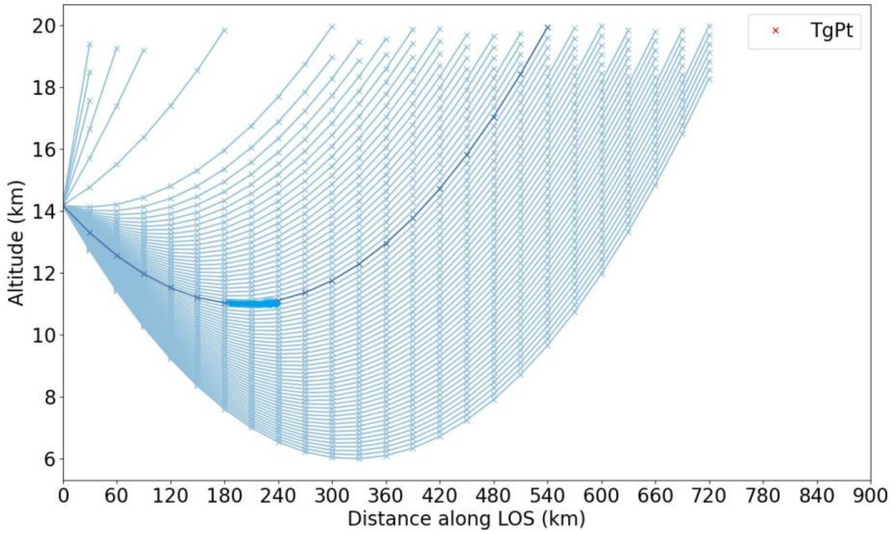

15. Figure 2: What happens when a cloud is present at high distances from the plane, beyond the tangent, and is picked up by a line-of-sight that shoots low? For instance, a cloud located 600km away from the plane at 14km ASL could appear in the lowest line of sight. In that case, would the cloud be attributed a ~6km altitude, ie a 8km error? Is there a way to know whether that situation is frequent, i.e. to quantify the error in vertical distribution due to that uncertainty on the cloud position along the line of sight?

It is right that if a cloud is located at 14 km altitude and is picked up by the line of sight with a tangent point altitude of 6 km, the cloud will be attributed to 6 km. In principle, it is not possible to know how many times that situation has been encountered in our analysis of the WISE campaign data. There is however, a study that could serve as a reference for the uncertainty in the CTH derived from limb viewing instruments and to which the reader is referred in page 11, line 16. Kent et al. (1997) address the questions than can arise from using the limb technique and the assumptions done in the retrieval. To do so, they simulated SAGE II cloud measurements and studied the uncertainty in the CTH determination and possible error situations. As stated in this comment, the first error is that the true cloud might be located at a higher altitude than that of the tangent layer to which is attributed. In the study of Kent et al. (1997) about 60% of the simulations had no altitude error and under 40% showed an error of 1 km or greater.

16. Section 2.1: This might be painfully obvious to the authors, but I'm afraid I'm not sure I understand in which direction the scan is occurring? Are the lines of sight always pointing the same way with respect to the plane? Is the instrument looking in a different direction every time the plane changes direction?

GLORIA is always pointing to the horizon from the right side of the plane. There are three measuring modes. If the instrument is set in chemistry mode, then all lines of sights are 90°

(perpendicular to the flight trajectory). If the instrument is in premier or panorama or panorama mode, then it pans from 45° to 135° (with respect to the plane) in intervals of 4° and 2°, respectively.

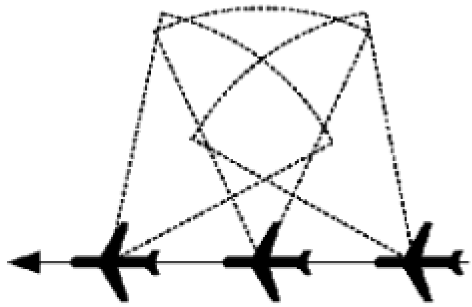

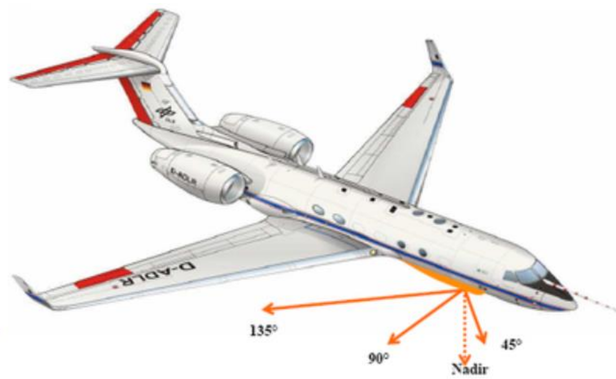

The paragraph in page 4, line 4-9 has been modified to make this point clearer:
"GLORIA always points towards the horizon from the right side of the plane. It is typically configured to one of three measuring modes: one high spectral resolution mode called chemistry mode (CM) and two modes, premier and panorama modes (DM), focusing on dynamical effects in the atmosphere. During CM, the instrument is fixed at 90° with respect to the flight trajectory. During the premier and panorama mode, the instrument changes its viewing direction between 45° and 135° in steps of 4° and 2°, respectively, which gives the possibility of observing the same volume of air from different perspectives and thus allowing for tomographic studies."

17. P. 9, Figure 3: Assuming I've understood correctly how to interpret GLORIA's measurements, does it mean that cloud base and top can be located very different distances away from the plane? Could you comment on whether this might impact the retrieved vertical distribution somehow?
If the observer is at 14 km, and the cloud top is assigned to the tangent point at 12 km and the cloud bottom at 10 km, that would mean a distance from the observer of about 150 km and 240 km, respectively. In the case of a homogenous cloud layer, this would not affect the vertical distribution. A more complicated case, are patchy clouds, but both cloud top and cloud bottom would be still relatively correct.

18. p. 9, L. 7: "the clouds were referred to the tangent point": Is this assumption made for convenience in absence of useful information, or is there a reason to think it is realistic? Is there a way to verify how frequently this assumption is reasonable or not, and quantify what the related uncertainty means for the cloud profiles?
In the retrieval technique applied to limb instruments, the inverse problem, necessary to retrieve the extinction from the measured radiance, is solved by dividing the atmosphere in spherical layers that are assumed homogenous, i.e. that the cloud would fill the complete layer:

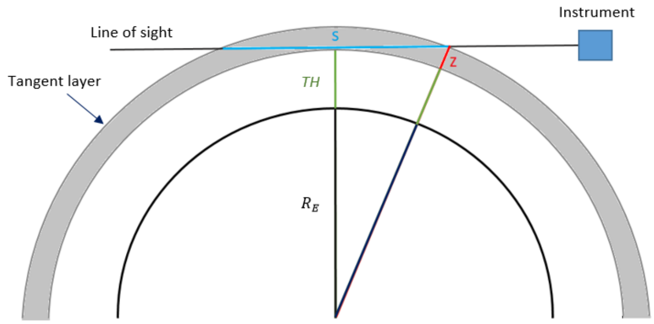

As discussed in comment 15, this assumption would lead to question the validity of the interpretation of the results (please, see answer to comment 15).

The leading error source in the determination of the cloud top, is the pointing knowledge along the LOS, which is about a tenth of a degree (Page 9, line 10-12). Other source are the oscillations in the extinction profile caused by the Gibbs phenomenon The Gibbs phenomenon describes the behavior of a Fourier series at a jump discontinuity, where an overshoot occurs and it does not disappear even if more terms are added to the Fourier sum. The overshoot, i.e. the radiance value larger than the maximum of the step function is of ≈ 10 %. At the edges of the function and after the overshoot, ringing artifacts, i.e small oscillations, appear. These effects can cause an error in the determination of the cloud top height of one grid point (± 125 m). These oscillations could also affect the determination of the cloud bottom, creating a false detection of a thin layer (1 – 2 pixels) above a thick cloud in ≈ 1 % of all the cloudy profiles. (Page 9, line 6-10).

19. Figure 3 and others: The WISE flights seem to cover a very large latitude range, from polar to almost tropical regions. Given we don't know where are clouds along the LOS, and what we know about the direction the LOS are pointing to, and the variable flight paths followed by the plane, is there a way to document the horizontal area described by these results?

As a reference, the location of the tangent altitude points has been included in the overview of scientific flights of the WISE campaign in Figure 1. The caption of Fig. 1 has been modified accordingly: "Overview of the 15 scientific flights of the WISE campaign. Color points correspond to the positions of HALO with GLORIA measuring. The red star indicates Oberpfaffenhofen, Germany and the red triangle Shannon, Ireland. The shade in light yellow gives a reference of the area covered by the measurements, indicating the distance of the tangent altitude point, i.e. of the closest point of the line of sight of the instrument to the surface."

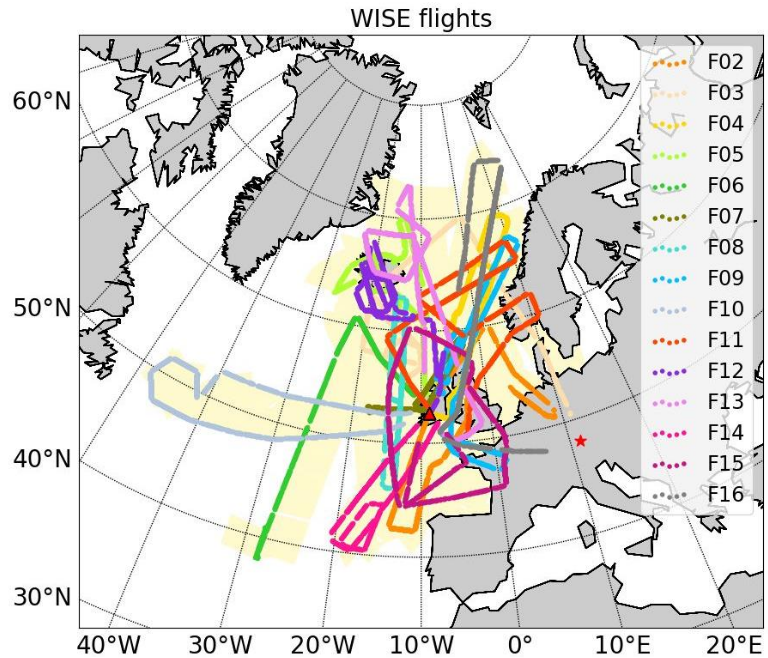

20. P. 10, Figure 5: could you add a figure showing the distribution of CI vs. Extinction? It could help quantify whether both variables are interchangeable.

Figure 5 has been modified to the following.

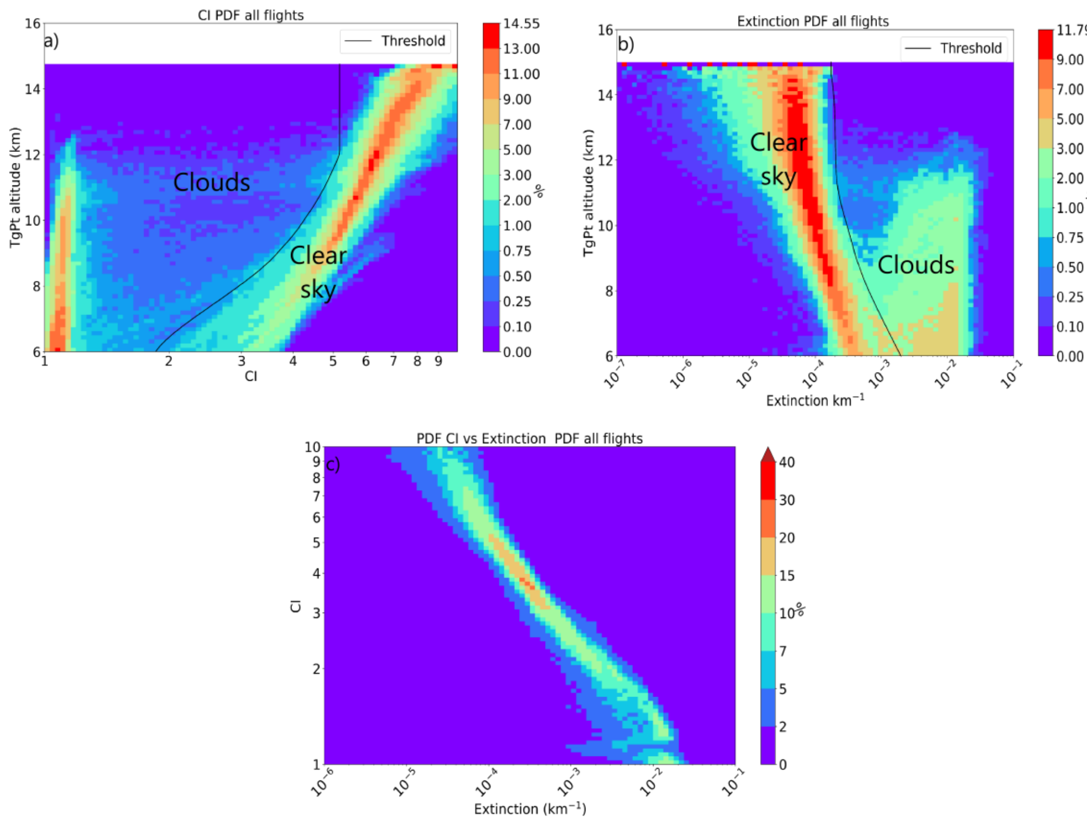

CI and extinction do not follow a one-one relation for the whole range, but for CI between 3 and 5, which would correspond to optically thin clouds (Spang et al., 2008), the relation is stronger (page 11, line 2-3).
Following the suggestion of referee 2, the percentage over all profiles that show a CTH for both methods is added in page 13, line 9-10. 61% of all profiles show a CTH for the extinction method, 59% for the CI and 58% for both methods. Therefore, they yield similar cloud identification results.

21. P. 12, L 26: "as discussed in Pan and Munchak (2011)..." The definitions of the tropopause are important, but the geographic colocation of the cirrus and the retrieved tropopause altitude is important as well. Given it is not possible to tell where a detected cloud is along the line of sight, it means there is an uncertainty of several hundred kms on the horizontal location of the detected cloud, with the largest uncertainties at the highest altitudes (closest to the tropopause). Trying to compare the altitude of a cirrus with the altitude of the tropopause when both can be separated horizontally by 600km makes me nervous, especially for clouds which are close to the midlatitude tropics boundary (where the tropopause can vary by several kms in a few hundred kms). Could you comment on the impact the cloud location uncertainty can have on colocating it with the tropopause, taking into account the latitude?
In order to take into account the variability of the tropopause along the line of sight, we decided to provide two altitudes for the tropopause: the median and the percentile 95 computed for each line of sight. The median would correspond to a more relax criteria, whereas the percentile 95 is a very conservative approach. Considering that the altitude of the determined cloud top could be lower than the true one (see answer to comment 15) if a cloud top is above the percentile 95, it gives us confidence enough to conclude that cloud tops were observed above the tropopause, despite the uncertainty in its exact location.

The following table is provided with the intention of giving a deeper insight into the variability of the tropopause for each flight, taking into account the maximum, the minimum, the median and the percentile 95. The maximum of the difference max – min (of all flights) is around 8 km, however, the median of the max-min is about 1 km for each flight, indicating that such a big difference is not often encountered.

	med(Max-min)	med(max-95)	med(95-med)	med(med-min)
F02	0.6	0.02	0.18	0.23
F03	0.8	0.02	0.23	0.43
F04	0.59	0.02	0.11	0.33
F05	1.02	0.05	0.34	0.44
F06	0.77	0.02	0.2	0.46
F07	1.28	0.03	0.5	0.6
F08	0.79	0.03	0.3	0.41
F09	0.9	0.02	0.35	0.45
F10	0.9	0.02	0.37	0.28
F11	0.39	0.02	0.16	0.17
F12	1.38	0.03	0.6	0.4
F13	1.02	0.04	0.37	0.32
F14	2.1	0.05	0.5	0.98
F15	1.05	0.02	0.46	0.41
F16	0.37	0.01	0.13	0.16
Mean(All flights	0.93	0.03	0.32	0.4
Max of max all	8.3	2.94	7.52	6.8
Min of min all	0.03	0	0.008	0.01

22. P. 13, Figure 7: Could you maybe plot the zonally averaged tropopause altitude on these plots?

We have added the mean tropopause height in coordinates of equivalent latitude to each plot in Figure 7. The tropopause has been computed from the ECMWF analysis data set, averaged over the duration period of the WISE campaign.

The caption of Figure 7 has been modified accordingly:

"PDFs of CTH as function of equivalent latitude (Eqlat) normalized for each altitude bin from (a) the extinction, (b) the CI and (c) ERA5 (discussed in Sect 4.3). The y axis shows the altitude of the tangent points (TgPt). The black line represents the mean tropopause height during September-October 2017 as a function of the equivalent latitude. It was computed from ECMWF analysis data."

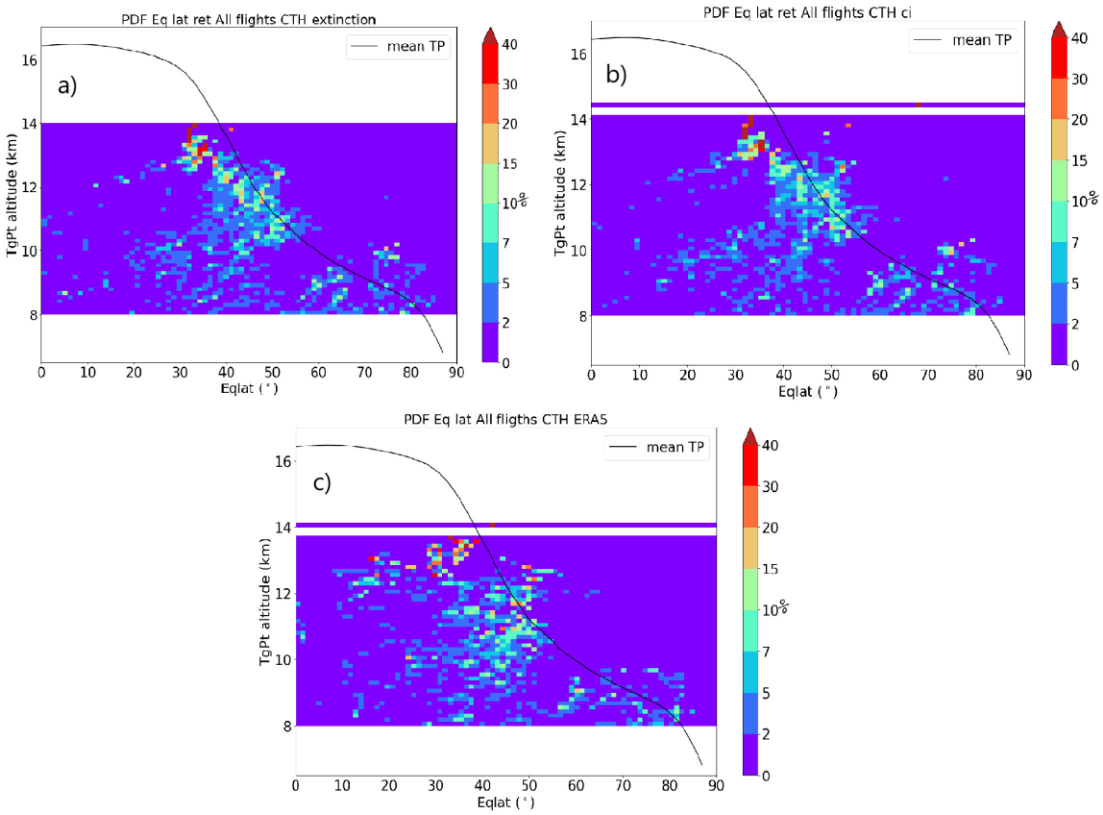

23. P. 14, Figure 8: Would it be possible to separate the distribution of cloud properties depending on whether the clouds were observed in tropical, midlat or polar latitudes? I would expect the vertical extents to vary with latitude.

The range of latitudes of the measurements covers from about 35°N to 75°N, which should not be mistaken with the equivalent latitude range than extends from 0°N - 90°N. The following plots correspond to the vertical extent of clouds in four latitude bands: [30-45)°N, [45-55)°N, [55-65) °N and [65-80] °N, for both detection methods. The latitude corresponds to the latitude of the tangent altitude point to which the CTHs are referred. N indicates the total number of CTHs, whereas n indicates the number of CTHs in the selected latitude band. The percentage is computed over N.

Most of the CTHs are located in the band 45-65°N and shifted towards vertical extension < 1.5 km.

We consider that these new plots look similar to the original Fig.8. Therefore, we have not modified Fig. 8 and we have added in page 15, line 6 that the latitude band with the largest number of CTH is between 45-65°N.

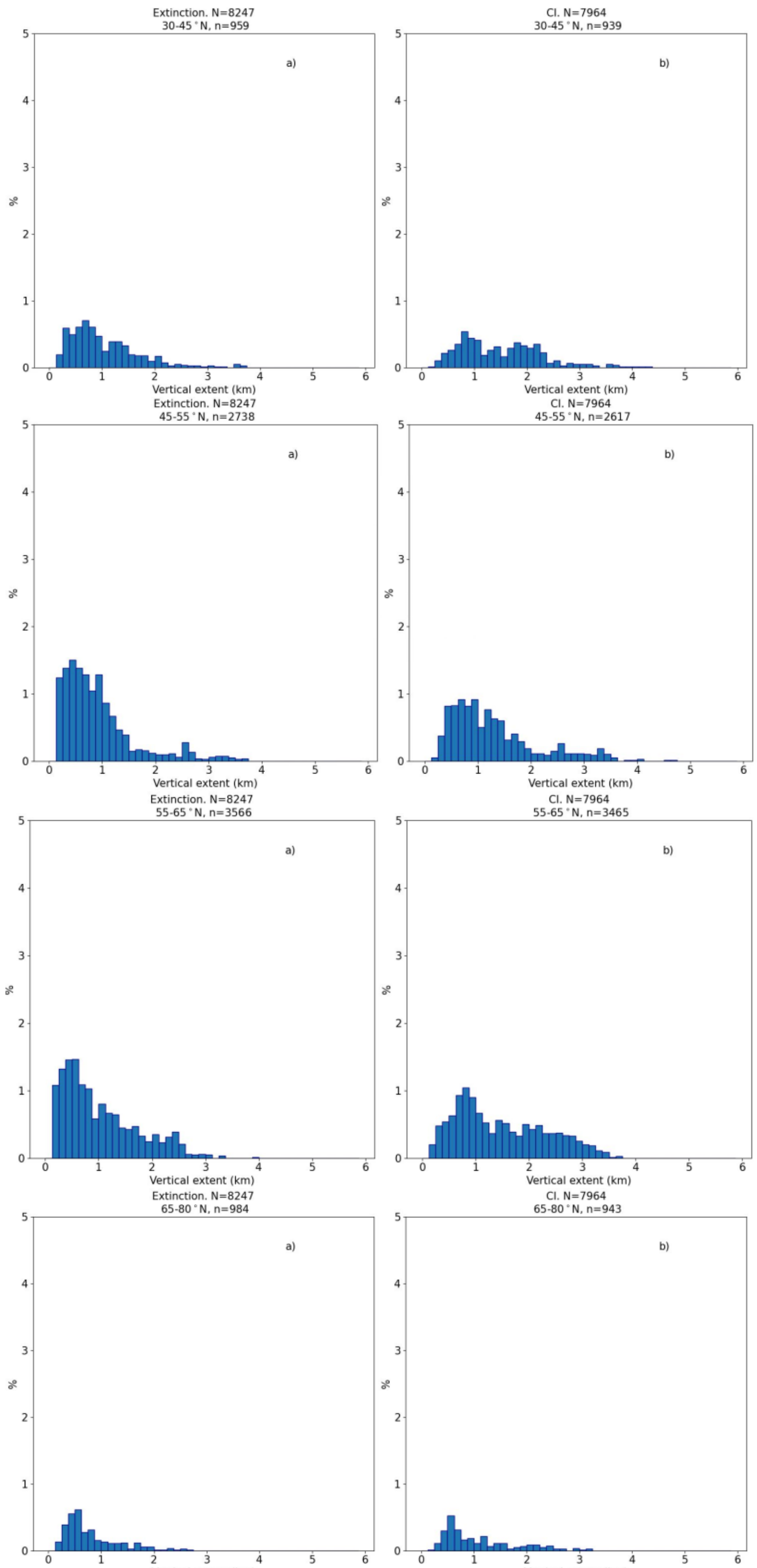
Extinction. N=8247
30-45 °N, n=959
a)
Cl. N=7964
30-45 °N, n=939
b)
Extinction. N=8247
45-55 °N, n=2738
a)
Cl. N=7964
45-55 °N, n=2617
b)
Extinction. N=8247
55-65 °N, n=3566
a)
Cl. N=7964
55-65 °N, n=3465
b)
Extinction. N=8247
65-80 °N, n=984
a)
Cl. N=7964
65-80 °N, n=943
b)
%
Vertical extent (km)

24. P. 14, L.5-6: "Spang et al..." this has already been stated close to the introduction. Please avoid repetition.

The sentence in question is the following: 'Spang et al. (2015) analyzed CRISTA data (Spang et al., 2015) and concluded with a frequency of occurrence of 5% of all observations and Zou et al. (2020) obtained 2% for CALIPSO data and 4 – 5% for MIPAS data.'

In the introduction the sentence is: 'A recent study with the Michelson Interferometer for Passive Atmospheric Sounding (MIPAS) and Cloud-Aerosol Lidar and Infrared Pathfinder Satellite Observations (CALIPSO) by Zou et al. (2020) finds that CALIPSO observes occurrence frequencies of about 2% of stratospheric cirrus clouds at mid and high latitudes and 4 – 5% for MIPAS in middle latitudes.'

We consider this repetition to be justified. In the introduction is used to give context to this study and further in the article to compare our results with their results, without needing to go back to the intro. We have included the results of these others studies in Table 2 to facilitate the comparison between results.

The sentence in question refers twice to Spang et al. (2105) and one of the references has been omitted (Page 16, line 26).

25. P. 15, Figure 10: I'm not sure I understand what is to be learned from these figures. If I understand correctly, they show the spatial distribution of detected cloud tops. Are we supposed to compare the left figure that shows all CTH with the right figure that shows only the CTH above the tropopause, and infer the regions where CTH above tropopause occur most frequently? If that is the case: 1) why change the color code between both figures? It makes the comparison much harder. Is the color code showing another point of comparison, or another independent information? 2) Isn't there an easier way to represent the density of CTH above the tropopause relative to the total number of measurements? (Eg counting the number of cloud points in 1x1° or 2x2° boxes?) 3) why isn't that discussed in the text? I don't understand how Figure 10 relates to what is discussed P. 13 lines 8-12.

The intention of figure 10 is to show the distribution of CTHs during the WISE campaign (a) and the distribution of the CTHs above the tropopause (b). Following the suggestion, we have changed the color code, so both figures have the same information (altitude of the CTHs). Figure 9 gives the occurrence frequency of CTHs above the median tropopause relative to the total number of observation.

We have modified the discussion about Fig. 10:

"Figure 10 shows the distribution of all CTHs (Fig.10) and the distribution of CTHs above TP_{med} for the extinction method. As can be seen, most of the occurrences of CTHs above TP_{med} were found between 50-70°N, with varying altitudes from 8-13 km. The few occurrences between 35-50°N were located at higher altitudes, from 10-14 km." (Page 16, lines 15-18)

26. P.16, L. 12: The already stated CALIPSO references (Martins and Reverdy) show a larger frequency of SVC and focus on the Tropics, it might make sense to refer to them.

We consider that introducing these references in the suggested section, i.e, comparison of GLORIA with ERA5, would affect the story line. We have added a reference to these studies in the introduction, where we can give an overview of the knowledge about SVC also in the tropics.

‘Detection of optically thin cirrus clouds and SVCs is a challenge due to the needed high vertical resolution and high sensitivity. Martins et al. (2010) analyzed CALIOP measurements over 2.5 years and gave an insight into the global frequency of SVC, being more common in the tropics (30-40%). Reverdy et al. (2012) reported a significant population of SVC in the tropical upper troposphere. However, Davis et al. (2010) found that CALIPSO would be missing about 2/3 of SVCs with $\tau < 0.01$ Due to the long path of the line-of-sight through the cirrus, typical of limb instruments, clouds that might be invisible to the nadir viewing instruments, are detectable. Spang et al. (2008) detect optically thin clouds with ice water content (IWC) down to 0.01 ppmv using the airborne limb instrument...’ (Page 2, 25-29).

Observation of Cirrus Clouds with GLORIA during the WISE Campaign: Detection Methods and Cirrus Characterization

Irene Bartolome Garcia[1], Reinhold Spang[1], Jörn Ungermann[1], Sabine Griessbach[2], Martina Krämer[1], Michael Höpfner[3], and Martin Riese[1]

[1]Institute für Energie and Klimaforschung (IEK-7), Forschungszentrum Jülich GmbH, 52428 Jülich, Germany
[2]Jülich Supercomputing Centre (JSC), Forschungszentrum Jülich GmbH, 52428 Jülich, Germany
[3]Institute of Meteorology and Climate Research, Karlsruhe Institute of Technology, 76021 Karlsruhe, Germany

Correspondence: Irene Bartolome Garcia (i.bartolome@fz-juelich.de)

Abstract. Cirrus clouds contribute to the general radiation budget of the Earth, playing an important role in climate projections. Of special interest are optically thin cirrus clouds close to the tropopause due to the fact that their impact is not yet well understood. Measuring these clouds is challenging as both high spatial resolution as well as a very high detection sensitivity are needed. These criteria are fulfilled by the infrared limb sounder GLORIA (Gimballed Limb Observer for Radiance Imaging of the Atmosphere). This study presents a characterization of observed cirrus clouds using the data obtained by GLORIA aboard the German research aircraft HALO during the WISE (Wave-driven ISentropic Exchange) campaign in September/October 2017. We developed an optimized cloud detection method~~and~~, based on the cloud index and the extinction coefficient retrieved at the microwindow 832.4-834.4 cm^{-1}. We derived macro-physical characteristics of the detected cirrus clouds such as cloud top height, cloud ~~top~~ bottom height, vertical extent and cloud top position with respect to the tropopause. The fraction of cirrus clouds detected above the tropopause is in the order of 13 % to 27 %. In general, good agreement with the clouds predicted by the ERA5 reanalysis ~~data-set~~ dataset is obtained. However, cloud occurrence is ≈50 % higher in the observations for the region close to and above the tropopause. Cloud bottom heights are also detected above the tropopause. However, considering the uncertainties, we cannot confirm the formation of unattached cirrus layers above the tropopause.

1 Introduction

High clouds, composed of ice crystals, are formed in the upper troposphere, where the temperatures are lower than -30°C. ~~It is possible to differentiate three genera: cirrus, cirrocumulus and cirrostratus. The first one consists of white delicate filaments, the second one of banks of small, white flakes and the third one of translucent cloud veils.~~ According to Sassen et al. (2008), these high clouds cover 16.7 % of the Earth's surface on average. All these clouds (from now on simply cirrus) are important, due to their frequent occurrence and their effect on the radiative budget of the Earth (Liou, 1986). Cirrus clouds ~~are rather transparent to incoming solar radiation, but absorb IR radiation from below and emit less to space due to the low temperature~~

of their environmentgenerally have a strong infrared greenhouse effect, leading to warming. However, optically thick cirrus with ice crystals of a few micrometers, can have the opposite effect (Krämer et al., 2016). Thus, they influence the amount of solar radiative energy received and also the loss of energy. These clouds are challenging to measure, because they can appear in multilayered cloud systems and they can be optically very thin, which complicates its detection by nadir sounders that are the typical operational weather satellitestheir detection by active as well as passive nadir sounders. Whereas in-situ measurements are capable of detecting the thinnest clouds, they only capture a temporally and spatially limited snapshot. Because of these difficulties, and despite being the subject of many studies, processes related to cirrus clouds are still not well understood and cause large uncertainties in climate projections (IPCC, 2013). Important factors influencing these uncertainties are ice water content, crystal number concentration and size distribution (Fusina et al., 2007). Other important factors that are problematic to determine are exact altitude and thickness. According to Sassen and Cho (1992) cirrus clouds are defined as (optically) thick for an optical depth $\tau > 0.3$, (optically) thin for $0.03 < \tau < 0.3$ and subvisible (SVC) for $\tau < 0.03$ in the visible wavelength region.

Of special interest is the effect of cirrus clouds in the upper troposphere / lowermost stratosphere (UTLS) region. Even small changes in the concentration of water vapor in this region affect the radiative forcing of the atmosphere (Riese et al., 2012). The presence of cirrus clouds above the tropopause, that will evaporate as soon as they experience a temperature increase and thus contribute to the water vapor budget, is still an ongoing discussion. Pan and Munchak (2011) show the importance of the employed tropopausedefinition and usage of tropopause relative coordinates for this kind of analysis. Using the same set of measurements from the Cloud and Aerosol Lidar While Dessler (2009) indicated the existence of a substantial amount of cirrus clouds above the tropopause, Pan and Munchak (2011), using the same Cloud-Aerosol Lidar with Orthogonal Polarization (CALIOP) as Dessler (2009), they find less occurrences data, demonstrated that the amount of cirrus clouds above the tropopause and consider strongly depends on the definition of the tropopause. Moreover Pan and Munchak (2011) concluded that there is not enough evidence of clouds above the tropopause in mid-latitudes. Spang et al. (2015) use A follow up study by Spang et al (2015), using the measurements from the Cryogenic Infrared Spectrometers and Telescopes (CRISTA) and ERA-Interim temperature fields for the determination of the local tropopauseand conclude , concluded that there is a significant number of occurrences in the lowermost stratosphere at mid and high latitudes. A recent study with the Michelson Interferometer for Passive Atmospheric Sounding (MIPAS) and Cloud-Aerosol Lidar and Infrared Pathfinder Satellite Observations (CALIPSO) by Zou et al. (2020) finds that CALIPSO observes found that CALIPSO observed occurrence frequencies of about 2 % of stratospheric cirrus clouds at mid and high latitudes and 4 – 5 % for MIPAS in middle latitudesat mid-latitudes (six year mean global distribution 2006-2012). Other studies based on measurements by ground-based LIDARs lidars show thin cirrus that are unambiguously located in the lowermost stratosphere (Keckhut et al., 2005). In the analysis of Goldfarb et al. (2001) using data from northern mid-latitudes, cirrus cloud tops often occur at the tropopause and SVC constitute 23 % of the total occurrences of cirrus clouds.

Detection of optically thin cirrus clouds and SVCs is a challenge due to the needed high vertical resolution and high sensitivity. This type of clouds is often invisible to nadir viewing instruments, but detectable by limb viewing instruments due to the longer Martins et al. (2011) analyzed CALIOP measurements over 2.5 years and gave an insight into the global occurrence of SVCs, being more common in the tropics (30-40 %). Reverdy et al. (2012) reported a significant population of SVCs in the tropical upper troposphere. However, Davis et al. (2010) found that CALIPSO would be missing about 2/3 of SVCs with $\tau < 0.01$. Due to the long path of the line-of-sight (LOS) through the cirrus~~. Spang et al. (2008) detect~~ , typical of limb instruments, clouds that might be invisible to the nadir viewing instruments, are detectable. Spang et al. (2008) detected optically thin clouds with ice water ~~content~~ contents (IWC) down to 0.01 ppmv using the airborne limb instrument Cryogenic Infrared Spectrometers and Telescopes for the Atmosphere - New Frontiers (CRISTA-NF). This IWC ~~value~~ matches the lower limit of the expected IWC for mid-latitude cirrus clouds 0.01 – 200 ppmv (Luebke et al., 2016). Our study uses data from the airborne Gimballed Limb Observer for Radiance Imaging of the Atmosphere (GLORIA) instrument (Riese et al., 2014; Friedl-Vallon et al., 2014). This instrument possesses the technical characteristics necessary for the detection of thin cirrus and SVCs. It has a spatial ~~resolution~~ sampling of 140 m $\times$ 140 m (horizontal sampling $\times$ vertical sampling) at a tangent point altitude ~~of~~ (i.e. closest point of the LOS to the Earth's surface) of 10 km for a flight altitude of 15 km. It measures in the infrared spectral region between 780 and 1400 cm^{-1} and its long ~~line-of-sight~~ LOS provides sufficient sensitivity to low ice concentrations. The mid-IR radiative properties of cirrus clouds depend on particle size, particle shape and the considered wavelength (Baran, 2005; van de Hulst, 1958; Yang et al., 2001). For this study, the configuration of the retrieval of the extinction coefficient is fixed for the microwindow 832.4-834.4 cm^{-1}.

Our work analyzes the cirrus measured by GLORIA during the Wave-driven ISentropic Exchange (WISE) campaign in September/October 2017 with the purpose of obtaining more information about the nature of cirrus ~~and~~ (both macro-physical and micro-physical properties) and thus, improve the understanding of their formation processes. The analysis includes the macro-physical properties of cirrus clouds, i.e., cloud top height (CTH), cloud bottom height (CBH), vertical extent and their position with respect to the tropopause. The tropopause was computed following the definition of the first thermal tropopause from WMO (1957).

2 Datasets and instrument

2.1 The instrument: GLORIA

GLORIA is part of the heritage of CRISTA-NF, which was a limb viewing airborne instrument with a vertical resolution of 200 – 400 m and two spectrometers with spectral resolution of $\approx$2 cm^{-1} and $\approx$ 1 cm^{-1}, respectively. This instrument represented an important ~~step~~ stepping stone toward future remote sensing limb instruments with even higher vertical and horizontal resolution. The GLORIA instrument and the data processing chain is described in previous studies, therefore the reader is referred to the works of Kleinert et al. (2014), Friedl-Vallon et al. (2014), Riese et al. (2014) and Ungermann et al. (2015) for a more detailed description. Here the main concepts are presented.

GLORIA is an infrared limb emission sounder that combines the Fourier-transform spectroscopy with a 2D infrared detector and measures radiances in the ~~mid-infrared~~ mid-IR range (780 – 1400 cm^{-1}). It was designed with the purpose of providing information about trace gases and temperature fluctuations in the observational gap that comprises small-scale structures of less than 500 m of vertical extent and less than 100 km in the horizontal. With GLORIA, it is possible to retrieve the distribution of different trace gases and aerosols, reconstruct gravity waves and study clouds in the UTLS (e.g. Blank, 2013; Krisch et al., 2018; Höpfner et al., 2019). The high spatial resolution, 140×140 m (horizontal sampling × vertical sampling) at a tangent point altitude of 10 km and observer altitude of 15 km, and the high precision sensors to obtain a good pointing accuracy, make GLORIA a perfect instrument for ~~measuring~~ investigating optically and vertically thin cirrus. The instrument is typically configured to use 48×128 pixels of its 2D detector array. As the main focus of this study is the characterization of cirrus clouds close to the tropopause and thus the most important feature is the vertical resolution, we do not analyze each individual pixel, but the horizontally averaged spectrum (averaged over 48 pixels) of each line of the 2D array. The final result is one profile for each measured set of interferograms with 128 spectra. The amount of radiance that each pixel receives is determined by the point spread function (PSF). The shape of the PSF is approximated by an Airy-disk with an aperture of ~~2.01~~the instrument of 3.6 cm and using 830 cm^{-1} as a reference wavelength. This configuration has been computed from a theoretical set-up of the instrument and was validated by cloud top measurements. The vertical sampling is higher the closer the tangent point altitude is to the observer altitude, as the projection of the PSF gets wider the further the tangent point is. For example, if the observer altitude is 14.7 km, at a tangent point of 13 km, the vertical sampling is about 88 m, at 10 km it is about 150 m and at 8 km it is about 179 m.

GLORIA always points towards the horizon from the right side of the plane. It is typically configured to one of three measuring modes: one high spectral resolution mode called chemistry mode (CM) and two modes, premier and panorama modes (DM), focusing on dynamical effects in the atmosphere. During ~~the~~ CM, the instrument is fixed at 90° with respect to the flight trajectory. During the premier and panorama mode, the instrument changes its viewing direction between 45° and 135° in steps of 4° and 2°, respectively, which gives the possibility of observing the same volume of air from different perspectives and thus allowing for tomographic studies. This capability of GLORIA ~~is~~ was used for the reconstruction of gravity waves (Krisch et al., 2018) and clouds (Ungermann et al., 2020). Table 1 summarizes the most important technical ~~characteristics~~ features of GLORIA. The data processing chain of GLORIA consists of three stages: the raw data processing (level 0), the processing into geolocated calibrated spectra (level 1) and the retrieval of geophysical quantities leveraging the fast radiative transfer model JURASSIC2 (section 2.4) (Hoffmann et al., 2008; Griessbach et al., 2013; Ungermann et al., 2015). This work uses level 1 and level 2 products.

2.2 The campaign: WISE

The data analyzed in this study ~~was~~ were measured during the WISE (Wave-driven ISentropic Exchange) campaign. It took place in Shannon, Ireland (52.70°N, 8.86°W) in September and October of 2017. With a total of fifteen scientific flights (plus a first test flight) (Fig. 1) covering the North Atlantic area, it aims to answer questions related to mixing, the role of Rossby wave breaking events in the transport of trace gases, such as water vapor, the formation of cirrus clouds and several other topics (Riese et al., 2017, last accessed: 13 August 2020). All the measurements were taken onboard the German research aircraft HALO (High Altitude and Long Range Research Aircraft), where GLORIA was placed in the belly-pod. HALO can fly to a maximum altitude of 15 km, which means that the vertical coverage of GLORIA observations during this campaign ~~ranges~~ ranged from ∼15 km down to ∼5 km.

Table 1. Instrument specifications (Friedl-Vallon et al., 2014). Observer altitude of 15 km and tangent altitude of 10 km. *Ungermann (2021, in prep.)(Ungermann, 2021, in prep.)

Property	Value
Temporal sampling	2 s (≈0.5 km)/12.8 s (≈3.2 km) for DM/CM
Spectral coverage	780 – 1400 cm^{-1}
Spectral sampling	0.0625 cm^{-1} to 0.625 cm^{-1}
Detector array size	256 × 256 pixels
Used detector array size	48 × 128 pixels
Vertical sampling	0.031°, equal to 140 m
Horizontal sampling	0.031°, equal to 140 m
Vertical spatial coverage	-3.3° below horizon to 0.8° above horizon
Horizontal spatial coverage	1.5°(=48 × 0.031°) equal to 6.7 km
Yaw pointing range	45° to 135°
Pointing precision (vertical)	0.012°, equal to ≈50 m (1σ)
*Pointing accuracy	0.1°

2.3 Meteorological dataset

We used the high resolution ERA5 data-set dataset provided by the European Centre for Medium-Range Weather Forecasts (ECMWF). The reanalysis data are available at 31 km horizontal resolution at 137 levels from surface to 80 km (Hersbach et al., 2020). The ERA5 dataset provides hourly data for a large variety of meteorological and climate variables. To perform the comparison between model and measurements, the variables of interest were sampled according to the GLORIA measuring geometry, as shown in Fig. 2. This figure represents the limb geometry during one measurement. For every line-of-sight (LOS)LOS, every 30 km, the meteorological variables were computed from the corresponding parameters of the ERA5 data set, i.e. first thermal tropopause (TP), equivalent latitude and ice water content (IWC)., i.e, the cloud ice mass in unit volume of atmospheric air. As the signal is integrated along the LOS of the instrument, the same applies for the IWC, thus the final parameter used for the comparison is was the limb ice water path (IWP), i.e. the IWC integrated along the LOS (Spang et al., 2015). In addition, we retrieved the potential vorticity (PV) and equivalent latitudes latitude from the ECMWF data at the tangent point. The static stability (N^2) used to analyze the stability of the atmosphere was computed from GLORIA retrievals. The potential temperature static stability is the square of the Brunt-Vaisala frequency (N), defined as:

$$N = \sqrt{\frac{g}{\theta}\frac{\partial\theta}{\partial z}}, \quad (1)$$

where g is the local acceleration of gravity, θ is the potential temperature, and z is the altitude of the air parcel. N^2 describes the vertical temperature stratification of the atmosphere and gives an insight of if an air parcel is in a transition region between

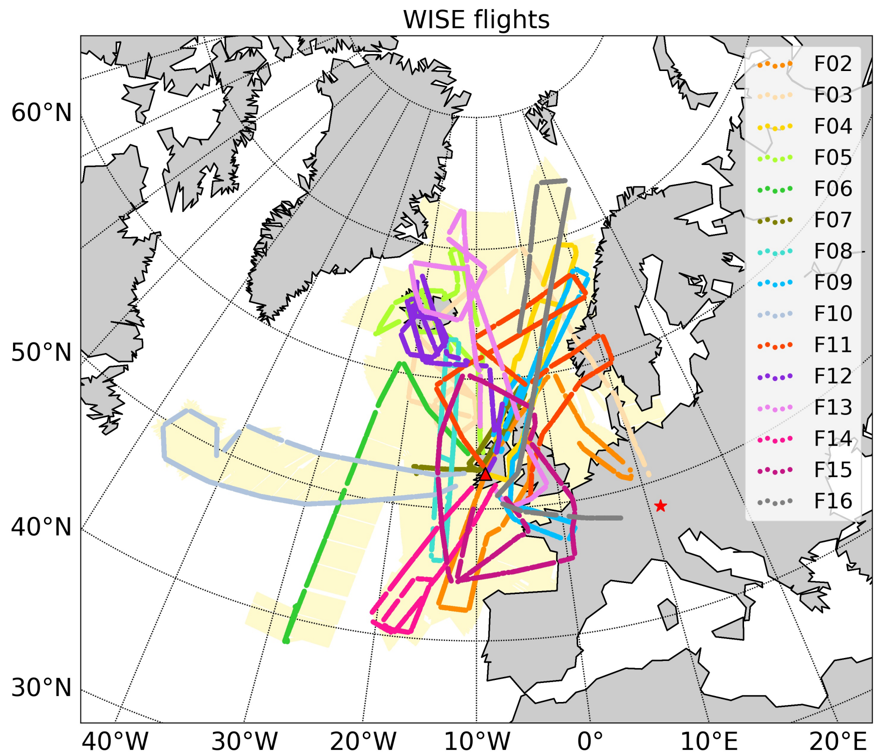

Figure 1. Overview of the 15 scientific flights of the WISE campaign. Color points correspond to the positions of HALO with GLORIA measuring. The red star indicates Oberpfaffenhofen, Germany and the red triangle Shannon, Ireland~~(NASA's Earth Observatory)~~. The shade in light yellow gives a reference of the area covered by the measurements, indicating the distance of the tangent altitude point, i.e. of the closest point of the LOS of the instrument to the surface.

the troposphere, characterized by low N^2 ($N^2 \approx 1 \times 10^{-4}$ s^{-2}) and the stratosphere, characterized by high N^2 ($N^2 \approx 5 \times 10^{-4}$ s^{-2}) (Grise et. al 2010).

The potential temperature product needed for the computation of N^2 was computed from pressure and temperature of the final data set, which contains the retrieval results and a priori information taken from ECMWF. The results are dominated by a priori in regions where no measurements are available, i.e., in or below thick clouds.

2.4 The model: JURASSIC2

The JUelich Rapid Spectral Simulation Code V2 (JURASSIC2) is a fast radiative transfer model developed at Forschungszentrum Jülich for analyzing the measurements of remote sensing instruments ~~(Hoffmann, 2006)~~(Hoffmann et al., 2008; Griessbach et al., 201

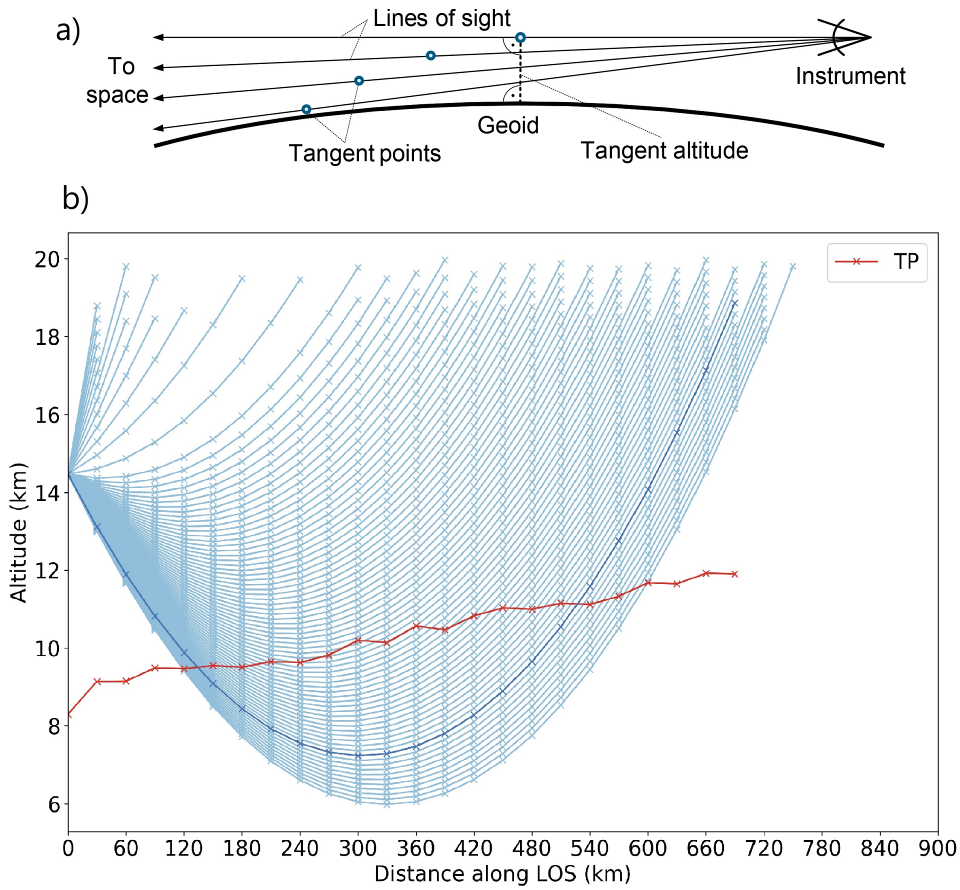

Figure 2. a) Example of the measuring geometry of GLORIA. The tangent altitude point is the closest point of the LOS (line-of-sight) to the surface. b) Example of the measuring geometry of GLORIA in a Cartesian system. Each blue line represents a different LOS that corresponds to a different elevation angle. The LOS is not a perfect straight line due to the refraction in the atmosphere and when plotted in a reference system with the Earth's surface as a straight line, it adopts a parabolic form. Each LOS is associated to a different tangent altitude. The horizontal distance of each LOS can extend several hundreds of kilometers. The lowest LOS are the ones with the largest path. The radiance measured by GLORIA is integrated along each LOS and contains the information related to the presence of clouds. The radiance from all lines of sight are recorded simultaneously. The red line indicates the tropopause (TP) from ERA5 along the corresponding ~~line-of-sight~~ ~~(~~LOS~~)~~, in dark blue.

. It combines a forward model with retrieval techniques ~~and~~ (for both limb and nadir geometries) and allows us to derive pressure, temperature and trace gas volume mixing ratios among others. JURASSIC2 solves the Schwarzschild Equation ~~in the mid-infrared~~ (Petty, 2006; Wallace and Hobbs, 2006) in the mid-IR region using spectrally averaged radiances, the Curtis-Godson Approximation (CGA; Curtis, 1952; Godson, 1953) and Emissivity Growth Approximation (EGA; Weinreb and

Neuendorffer, 1973; Gordley and Russell, 1981) in combination with emissivity look up tables (LUT) (Ungermann et al., 2011). The LUT are typically computed by the line-by-line Reference Forward Model (Dudhia, 2017).

JURASSIC2, together with the Juelich Tomographic Inversion Library (JUTIL), generates the level 2 products (temperature, trace gases, extinction coefficient). For a detailed description of this process the reader is referred to Ungermann et al. (2015). For this study, the level 2 product used is simply the extinction coefficient. An explanation of how it is retrieved is given in Sect. 3.2.

3 Cloud detection methods

To analyze the data, two methods to identify optically and vertically thin clouds at high altitudes were used~~, a~~. One method used the cloud index and the other the extinction coefficient.

3.1 Cloud index

The cloud index (CI) was first introduced by Spang et al. (2001) and has been widely used in different studies for the analysis of clouds in the UTLS and polar stratospheric clouds observed by CRISTA and MIPAS (Sembhi et al., 2012; Spang et al., 2015, 2016). The CI is a dimensionless number defined as the ratio between the mean radiances of two microwindows:

$$\frac{I(788.2-796.2)\mathrm{cm}^{-1}}{I(832.4-834.4)\mathrm{cm}^{-1}} CI = \frac{I_1([788.2, 796.2\mathrm{cm}^{-1}])}{I_2([832.4, 834.4\mathrm{cm}^{-1}])} \tag{2}$$

The first spectral window is mainly dominated by emissions of a CO_2 Q-branch and the second is an atmospheric window region. The CI is affected by the water vapor continuum contribution to the atmospheric window at low altitudes and depends slightly on latitude and season (Sembhi et al., 2012). When clouds are present, the emission in both ~~microwindow~~ microwindows increases. However, the relative increase in the CO_2 Q-branch is smaller. As a result, the ratio decreases, therefore ~~low values of CI indicate~~ a low CI indicates cloudy conditions. A $\sim 1.1 <$ CI < 4 indicates the presence of clouds (Spang et al., 2008, 2015).

3.2 Extinction coefficient retrieval

The extinction coefficient (from now on simply extinction) was retrieved with JURASSIC2. Although scattering by cloud particles has an impact on the measured radiance (Höpfner and Emde, 2005), we simulated the radiative transfer without scattering. As explained by Höpfner and Emde (2005) the difference between zero scattering and multiple scattering for a case that falls between the two cases presented in their study (ω_0 = 0.24 and ω_0 = 0.84), would be between 25-28 %. Additionally, we performed test runs with single scattering for two flights using the radiative transfer model JURASSIC2. ~~The difference~~ These flights were selected because both thin cirrus and thick cirrus were observed, and therefore, constitute an interesting case for studying the influence of scattering in different cases. The difference (calculated as the mean of the median difference of both flights) between the extinction neglecting scattering and the extinction including single scattering is 21 %, with 73 % as the percentile 95 and -86 % as the percentile 5 (results not shown). ~~We considered~~ The mean difference at 2σ, i.e percentile

16 and percentile 84 is -4 % and 49 %, respectively. For the retrievals with single scattering, the CTH was computed following the same procedure as for the retrievals with no scattering. For 98 % of all cases, both retrievals detected a cloud. The altitude of the CTH was for about 71 % of the detected clouds the same, being the typical difference 0-0.375 km. Following the same procedure for the CBH, for 90 % of all cases, both retrievals detected a CBH, obtaining the same altitude in 58 % of the coincidental profiles. The typical difference for the CBH was also 0 – 0.375 km. The detected clouds for both flights and both retrievals covered the range 45°N - 75°N, with the largest occurrence between 55°N – 75°N. In consideration of these results, we conclude that for our current purpose of obtaining macro-physical properties of cirrus clouds the non-scattering approach is sufficient.

Obtaining the extinction means solving an ill-posed inverse problem. In our inverse problem, there is a state vector $\boldsymbol{x}$ describing the state of the atmosphere (quantities to be retrieved), a measurement vector $\boldsymbol{y}$ with error $\boldsymbol{\epsilon}$, and a forward model $\boldsymbol{F}$ implementing the physics of the involved processes.

$$\boldsymbol{y} = \boldsymbol{F}(\boldsymbol{x}) - \boldsymbol{\epsilon} \tag{3}$$

For this work, $\boldsymbol{x}$ is the extinction and $\boldsymbol{y}$ is the radiance in the microwindow 832.4 – 834.4 cm^{-1}. This interval is the same one used for the CI. For a detailed explanation of the retrieval the reader is referred to Ungermann et al. (2015).

The retrieval grid consists of a constant altitude grid with 81 levels ranging from 6 km to 16 km with a sampling distance of 0.125 km. The model includes corrections of the tangent altitudes due to the elevation angle offset and the refraction. Several tests comparing the radiance of a theoretical case of a cloud as a step function and the retrieved one were performed to determine the influence of the radiance of cloudy pixels on the pixels above (not shown), i.e. the effect of the PSF. The results show that the retrieved profiles are affected by Gibbs oscillations that cause ringing artifacts at the edges and an overshoot of ≈10 % is found (i.e. radiance ~~value~~ larger than the maximum of the step function). These effects can cause an error in the determination of the cloud top height of one grid point (± 125 m). These oscillations could also affect the determination of the cloud bottom, creating a false detection of a thin layer (1 – 2 ~~pixels~~grid points) above a thick cloud in ≈ 1 % of all the cloudy profiles. The leading error term in the determination of the cloud top altitude is the pointing knowledge along the LOS. This error is about a tenth of a degree, which ~~has been~~ was validated by measurements of the Moon during several flights (Ungermann, 2021, in prep.).

The range of retrievable ~~extinction values for clouds~~ cloud extinctions is from about $2\times10^{-4}\,\mathrm{km}^{-1}$ to $4\times10^{-2}\,\mathrm{km}^{-1}$ and allows for the detection of optically thin cirrus, one of the objectives of this study. The upper limit is determined by the optical thick conditions in the limb direction and the lower limit by background aerosol and calibration uncertainties.

We sampled the CI on the extinction retrieval grid to allow for a comparison of both methods (Fig. 3). The radiative transfer model assumes for practical reasons a horizontal homogeneous atmosphere. As such, it assumes that simulated measurement rays diving below a cloud layer passes through the cloud twice, whereas in the actual situation it may 'miss' the cloud on both occasions; if this occurs, the retrieval assigns nonphysical low extinction ~~values~~ close to 0 to those regions (Fig. 3a, e.g. at 11:29 UTC, 11 – 12 km). Above the clouds (0.125-0.250 km), the low extinction is due to the second order regularization that smooths the profiles and causes Gibbs oscillations in the extinction profile at strong ~~value~~ extinction changes. For the CI cross-section (Fig. 3b), depending on the altitude, different CI threshold values indicate the presence of clouds. A detailed explanation about the detection threshold is found in Sect. 3.3.

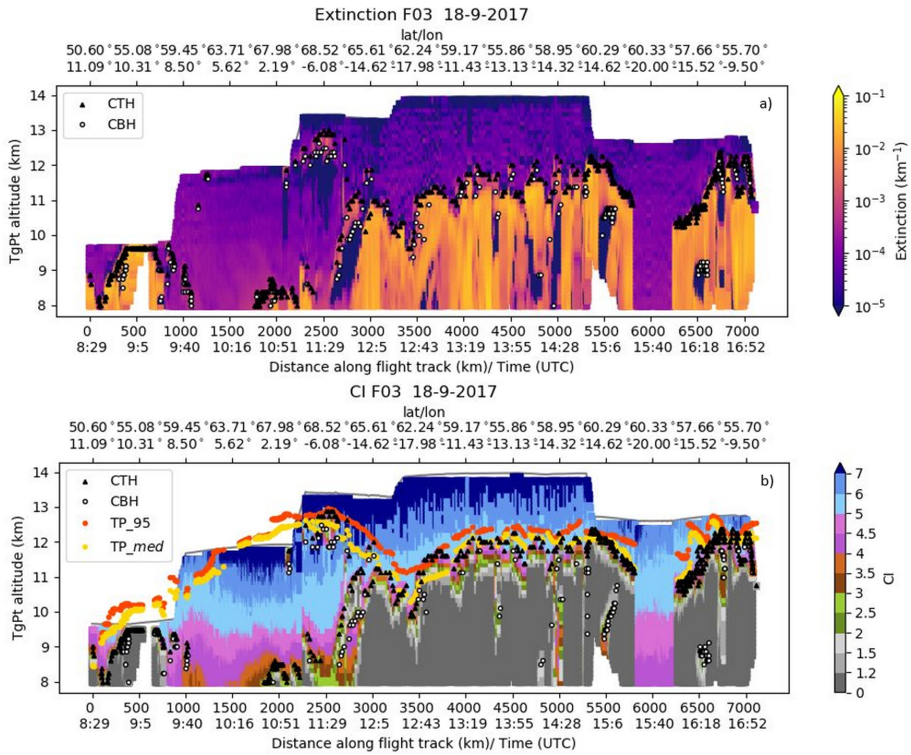

Figure 3. Cross-sections of extinction (a) and cloud index (b) for flight 3 of the WISE campaign. The results are restricted to levels below flight path. (a) Color code for extinction in km^{-1}. Orange-pink colors indicate the presence of clouds; (b) color code for CI. Depending on the altitude, CI ~~values~~ below 2 to 5 (colors from grey to pink) indicate the presence of clouds. Median tropopause (TP_{med}) and the percentile 95 of the tropopause (TP_{95}) are represented with orange and yellow circles, respectively. Cloud top height (CTH) and cloud bottom height (CBH) are represented with a black triangle and with a white circle, respectively. The altitude of the tangent points (TgPt) is the y axis. The white areas in both cross-sections correspond to a first filtering of optically thicker regions (CI < 2). These areas correspond to the tangent layers where the clouds are optically too thick.

3.3 Detection threshold for CI and extinction

To identify clouds in the measurements, we defined the detection thresholds for CI and extinction. First, we ~~define~~ defined the criteria for clear sky regions. As a first approximation of clear sky conditions, profiles with CI always greater than 2 and extinction always less than 10^{-3} km^{-1} were selected. From this first coarse pre-selection, the vertical extinction gradient (Fig. 4) was computed to have an automated method that is more sensitive to optically thin clouds. If this gradient has a small variability, that means there are no elements, i.e aerosols or cloud particles, that cause a sudden increase in the extinction and therefore a large gradient. Clear sky profiles were defined to be those with an extinction gradient lower than a threshold defined as the median extinction gradient of the pre-selected profiles of all flights together plus 5σ. A value of 5σ was chosen after a visual fit to the gradient to reduce the number of false detections to a minimum. It is possible that the aircraft flies inside a cloud, which causes the vertical gradient of the extinction to be approximately constant and thus considered as clear sky. To exclude these cases, the condition that the CI must always be greater than 2 was added. Below 8 km the extinction gradient increases, which indicates the influence of the water vapor continuum at low altitudes (Fig. 4). Therefore, the analysis was limited to the range from 8 km to the aircraft altitude. For all the clear sky profiles, PDFs probability density functions (PDFs) of CI and

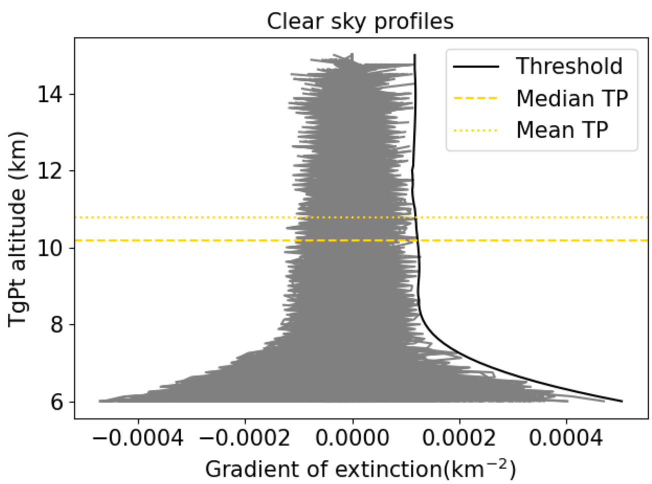

Figure 4. Clear sky profiles of the vertical Vertical gradient of the extinction coefficient for all flights togetherin the case of clear sky conditions. In black, the threshold defined as the median of the extinction gradient plus 5σ. Altitude of the tangent points (TgPt) in the y axis. The median tropopause height (Median TP) and the mean tropopause (Mean TP) height of all clear profiles is indicated by a dashed and a point yellow line, respectively.

extinction were calculated and normalized for each altitude bin. Using the PDF for guidance, a threshold for each parameter is was defined. The extinction coefficient threshold (k_{thres}) was defined as the median of the extinction plus 5σ. This threshold is sensitive to structures with very low extinction, down to $2 \times 10^{-4}\,\mathrm{km}^{-1}$ for a tangent point between $\sim$11.5 km and 15 km . This value (Fig. 5a, b). This detection limit is similar to the one provided by Sembhi et al. (2012) for MIPAS, with an extinction detection limit above 13 km of $10^{-4}\,\mathrm{km}^{-1}$ and to the findings of Griessbach et al. (2020), specified in Table 1 of the cited study. The CI threshold ($\mathrm{CI}_{\mathrm{thres}}$) is the percentile 1 (%) shifted by 0.3 (CI). Above 12 km we applied a constant CI value CI of 5 because there, the low number of counts observations and occurrences of clear sky shifts the threshold towards too high values of CI . This value, as well as the threshold for lower altitudes, CI numbers. Our threshold for this and lower altitudes agrees with the one defined by Sembhi et al. (2012) for northern mid-latitudes and Spang et al. (2012) for the MIPAS instrument. The threshold lines separate the clear air and cloudy cluster from each other, following the vertical gradient of the clear air cluster

(Fig. 5~~).~~ a, b). As seen in Fig. 5c, the relation between CI and extinction is not one-one. However, for CI between 3 and 5, which corresponds to optically thin clouds (Spang et al., 2008), the relation is stronger.

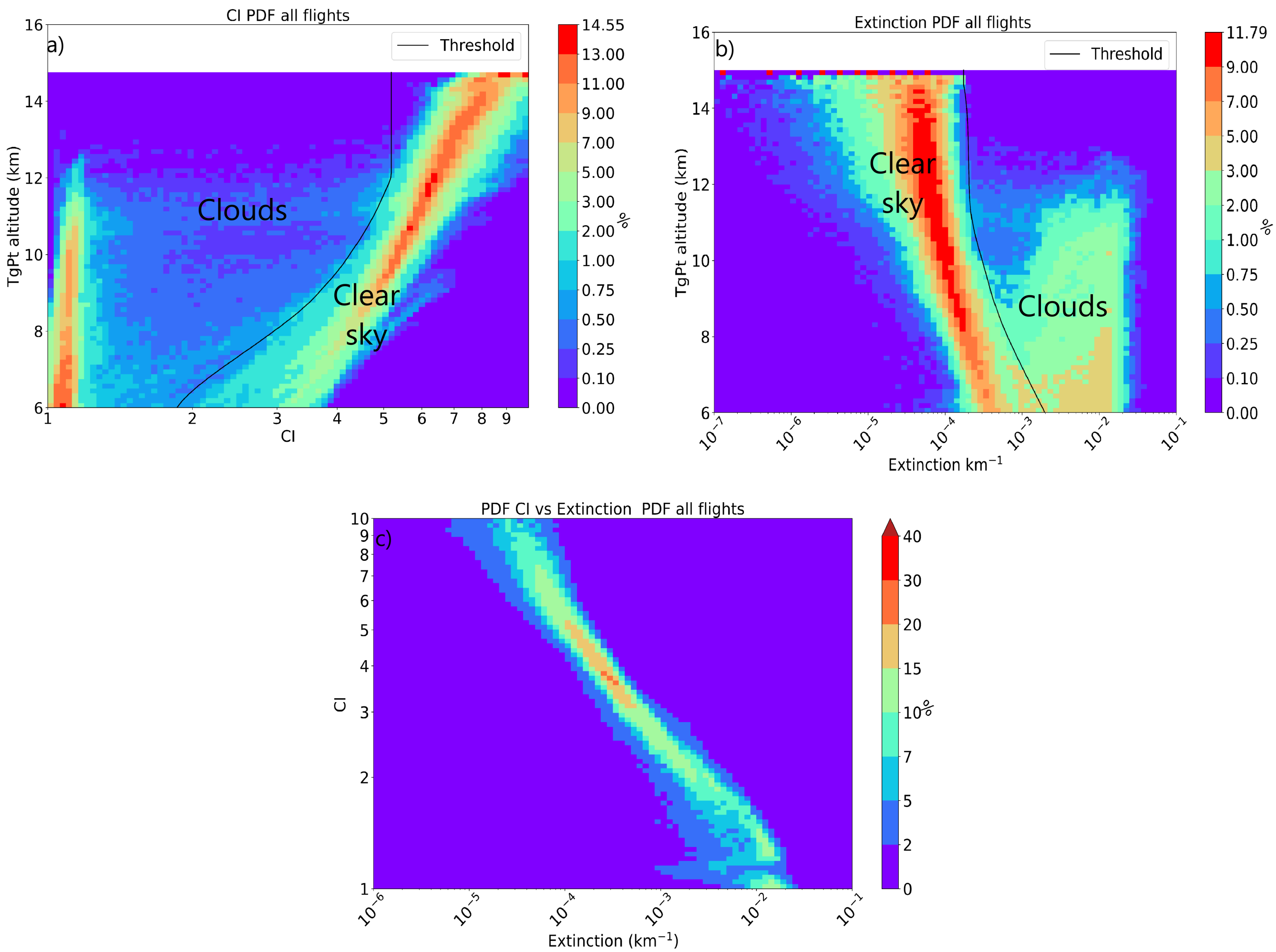

Figure 5. PDF for CI and extinction for all flights including all profiles. The bins are normalized by altitude. In black the threshold for differentiating cloudy conditions from clear sky. For (a) clouds correspond to small ~~values of~~ CI, i.e, the left side of the CI_{thres}. For (b) clouds correspond to high extinction~~values~~, i.e., to the right side of the k_{thres}. The altitude of the tangent points (TgPt) is the y axis. c) PDF of CI as a function of extinction, normalized by CI. The total number of analyzed profiles is 13539.

3.4 Definition of the macro-physical characteristics

Here, we define the macro-physical characteristics of the detected cirrus clouds that are presented in Sect. 4: cloud top height (CTH), cloud bottom height (CBH) and their vertical extent. In the limb geometry, the position of the cloud along the LOS is not exactly known. For analyzing the data, the clouds were referred to the tangent point, i.e., the point of the LOS closest to the Earth's surface and the corresponding tangent height layer. Using this definition of the position of the cloud, the CTH was defined as the first point in which the extinction (or CI) ~~has a value~~ is equal to or larger than the k_{thres} (or less than or equal to the CI_{thres}). For the analysis, we assumed a homogeneous cloud layer, which may underestimate the real extinction. This could cause an underestimation of the CTH for some cases, in which the cloud is on the ray path far from the tangent point location (Kent et al., 1997). All the CTHs belong to the first cloud detected, i.e., the analysis did not include multi-layer clouds (two or more clouds with a clear separation in between). The CBH of a cloud using the extinction method is the altitude of the first ~~point~~ detection in the series of limb observations with an extinction smaller than the k_{thres}; this ensures the identification of an altitude at or below the true cloud bottom. For the CI method, the CBH was computed using the minimum of the CI gradient of the profile (Kalicinsky et al., 2020). CBH could only be reliably determined for optically thin clouds. For optically thick conditions, the CI profiles saturate and the extinction profiles decrease in an unrealistic manner. Optically thick profiles are characterized by ~~CI-values~~ CI lower than 1.2 from an altitude h down to the lowest altitude (Spang et al., 2015, 2016). ~~Thin profiles~~Optically thin profiles, i.e with small extinction, are those for which it was possible to define a CBH. Figure 6 shows an example of a saturated CI profile and a profile for a cloud layer. It is possible to observe how the ~~saturated~~ CI profile reaches saturation ~~after CI =~~ for CI's smaller than 1.2. The last macro-physical characteristic that was analyzed is the vertical extent, defined as the CTH – CBH.

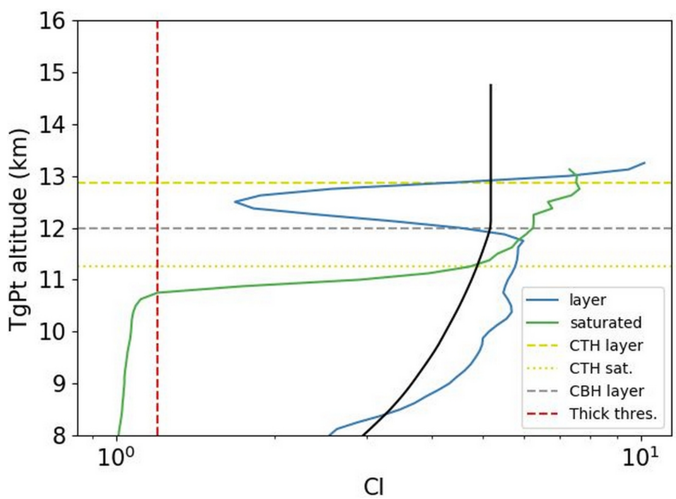

Figure 6. CI profile for a cloud layer (blue) and an optically thick case (green) that saturates. The horizontal yellow lines indicate the cloud top height (CTH) for the layer (dashed line) and the thick case (~~dashed point~~ points line). The horizontal dashed line in grey is the cloud bottom height (CBH) of the cirrus layer. The red vertical line corresponds to CI = 1.2 i.e. optically thick cases. In black, the CI threshold. The altitude of the tangent points (TgPt) is the y axis.

3.5 Differentiation between clouds and aerosol

Enhanced aerosol number densities can also affect the CI ~~values~~ and cause false cloud detection. To investigate if the presence of aerosol particles influenced the results, methods described by Griessbach et al. (2014) and Griessbach et al. (2016) were applied. These methods use the different ~~spectral slopes~~ wavelength dependence of ice and aerosols, such as volcanic ash or sulfuric acid, in five wavelength regions to establish thresholds that differentiate them. The results (not shown), indicated very little influence of these aerosols in our measurements.

4 Results

4.1 Analysis: cloud top height and cloud bottom height

During the WISE campaign, 61% of all observed profiles show CTHs using the extinction method and 59% for the CI. ~~These values~~ 58 % of all profiles show a CTH for both methods, which indicates a similar performance. These fractions are comparable to the climatology presented in Goldfarb et al. (2001) for lidar observations, with a cirrus occurrence frequency of 60% for fall. However, a fraction of 60% is considerably larger than the ≈17% reported by Sassen et al. (2008) for CALIPSO measurements and the International Satellite Cloud Climatology Project (ISCCP) for mid-latitudes. It is rather unlikely that this difference is related only to the disparate observational periods. We rather explain it by the differences in cirrus cloud selection criteria of the studies. While in our study there is no temperature threshold, Sassen et al. (2008) considered as cirrus only clouds with $\tau <\sim 3.0$ - 4.0 and with a maximum cloud top temperature of -40°C. Goldfarb et. al 2001 considered for the detection of cirrus a threshold that was defined for each nightly determination and required that the cloud layer was in an air mass with a temperature of -25°C or lower.

The extinction method and the CI method show good agreement in the determination of the CTHs, presenting a similar distribution (Fig. 7 a and b). The CTHs between 8 and 10 ~~km present~~ km were observed in air masses with equivalent latitudes that spread from tropical to polar regions, having a slightly higher frequency at the polar latitudes. ~~For~~ CTHs between 10 km and about 12.5 km ~~the air masses have an~~ often occurred at equivalent latitude typical ~~of~~ for mid-latitudes, whereas the ~~highest CTHs ,~~ CTHs above about 12.5 km ~~are almost subtropical~~ were related to subtropical latitudes. The main difference between both methods is ~~the~~ that the CTHs inferred from the CI are slightly higher (1 – 2 ~~pixels) CTHs of the CI~~ grid points) than for the extinction method.

~~Considering all observed profiles~~ From all considered profiles (13539), about 39 % ~~are~~ (5232 profiles) can be characterized as optically thick using the extinction method and 41 % (5517 profiles) the CI method. 36 % of all profiles are optically thick for both methods. The maximum extinction detected for thin clouds, in which a CBH was possible to determine, is $4 \times 10^{-2}\,\mathrm{km}^{-1}$.

The distribution of the vertical extent of clouds is presented in Fig. 8. The extinction method results in a higher amount of vertically thin clouds than the CI method, due to the slightly higher CBHs of the extinction method (Ungermann et al., 2020). For both methods, a large fraction of the optically thin cirrus clouds ~~have~~ were located between 45-65°N and had a vertical extent smaller than 1.5 km (31 % of the clouds detected with the extinction method and 20 % of the clouds detected

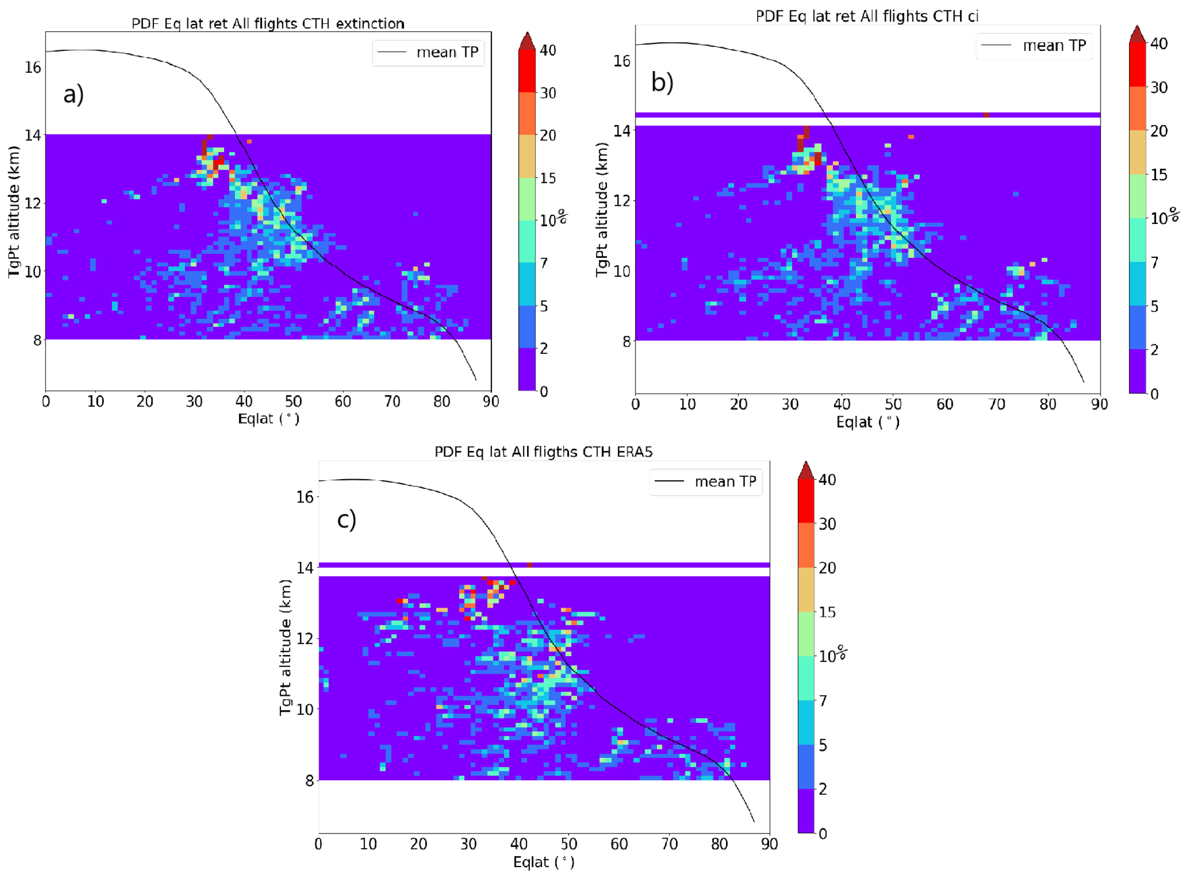

Figure 7. PDFs of CTH as function of equivalent latitude (Eqlat) normalized for each altitude bin ~~for~~ from (a) ~~CTH detected with~~ the extinction, (b) ~~CTH detected with~~ the CI and (c) ~~CTH from~~ ERA5, discussed in Sect. 4.3. The y axis shows the altitude of the tangent points (TgPt)~~is~~. The black line represents the ~~y axis~~mean tropopause height during September-October 2017 as a function of the equivalent latitude. It was computed from ECMWF analysis data.

with the CI method). These results are qualitatively similar to the findings of Noël and Haeffelin (2007). They ~~show~~ showed that between May and November the ~~vertical extent distribution~~ frequency distribution of the vertical extent of the observed clouds ~~is~~ was biased towards values between 0 and 1.5 km. Our results are also in agreement with the mean layer thickness of 1.4 km ~~computed~~ found by Goldfarb et al. (2001).

4.2 Cloud top position with respect to the tropopause

The occurrence frequency of cirrus clouds above the tropopause remains a matter of debate. The vertical resolution of the underlying temperature profile of the meteorological analysis for the tropopause computation is a key point for respective

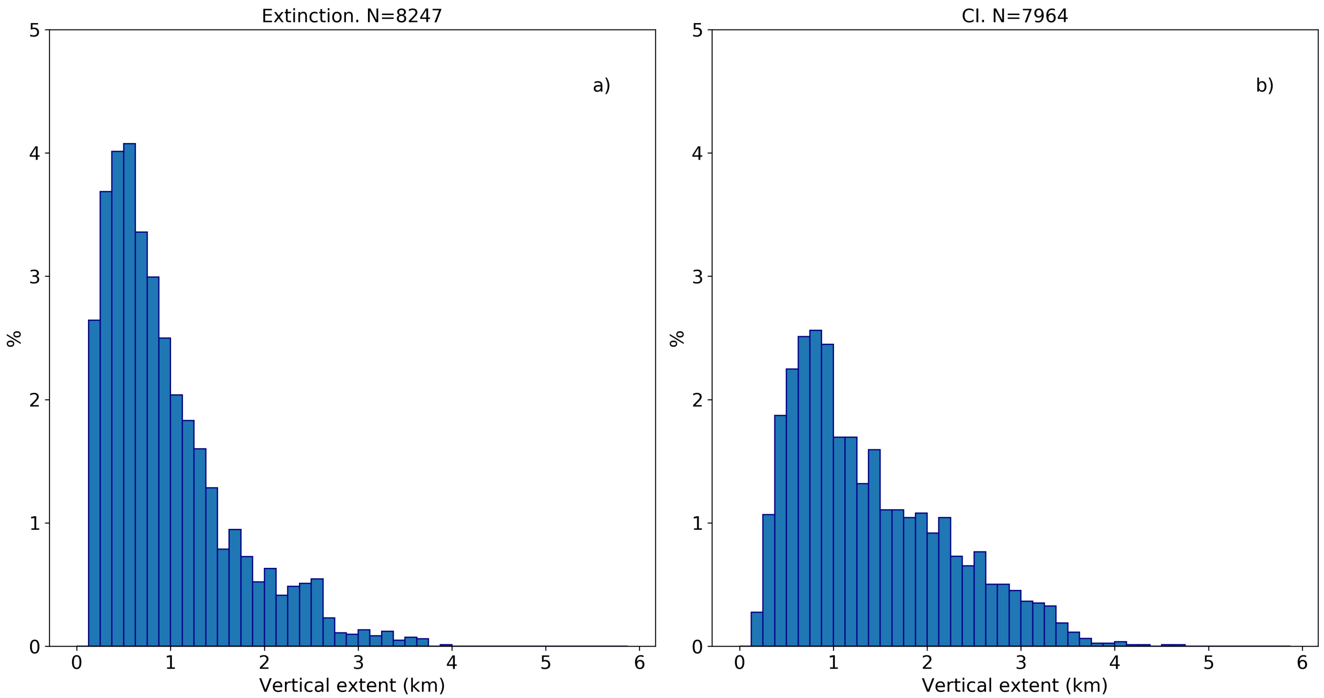

Figure 8. Distribution of the vertical extent of cirrus clouds for all flights for (a) the extinction method and (b) the CI method. The percentage is given in relation to the total number of CTHs (N) detected for each method.

analyses. As discussed in Pan and Munchak (2011) different definitions of the tropopause can lead to different results. For this study, the first thermal tropopause altitude was computed from ERA5 data. The LOS of GLORIA typically extends several hundreds of kilometers~~sampling air masses that can be heterogeneous. Consequently~~, hence the sampled air masses could be heterogenous in the horizontal. Further, the tropopause ~~is usually~~ height was not constant along the LOS (Fig. 2). Two methods were ~~applied~~ used for representative tropopause definition for the air mass sensed by the instrument: a) the median of the tropopause along the corresponding LOS of the CTH and b) the 95 % percentile. All extinction and CI cross-sections of the WISE campaign with CTHs, CBHs, median tropopause (TP_{med}) and 95 % percentile (TP_{95}) can be found in the supplement. Figure 3 illustrates the case of a flight with both homogeneous and heterogeneous air masses. E.g. the air mass at 16:18 UTC ~~is~~ was homogeneous and TP_{med} and TP_{95} are close to each other (less than 125 m apart). At 11:29 UTC, there ~~are~~ were heterogeneous air masses with TP_{med} and TP_{95} separated (three times the distance of the previous example), which affects the statistics of CTHs above the tropopause, since as to whether the CTH is located above or below the tropopause ~~depending~~ depends on the chosen tropopause altitude.

For the extinction method, the frequency of occurrence of CTHs above the TP_{med} is 24 % of the total number of observations, whereas for the CI method the ratio is 27 % (Fig. 9b). The $\approx$3 % difference is due to the CI detecting CTHs slightly higher than the extinction method. When considering TP_{95}, the percentages decrease to 13 % and 16 % respectively as it uses a more

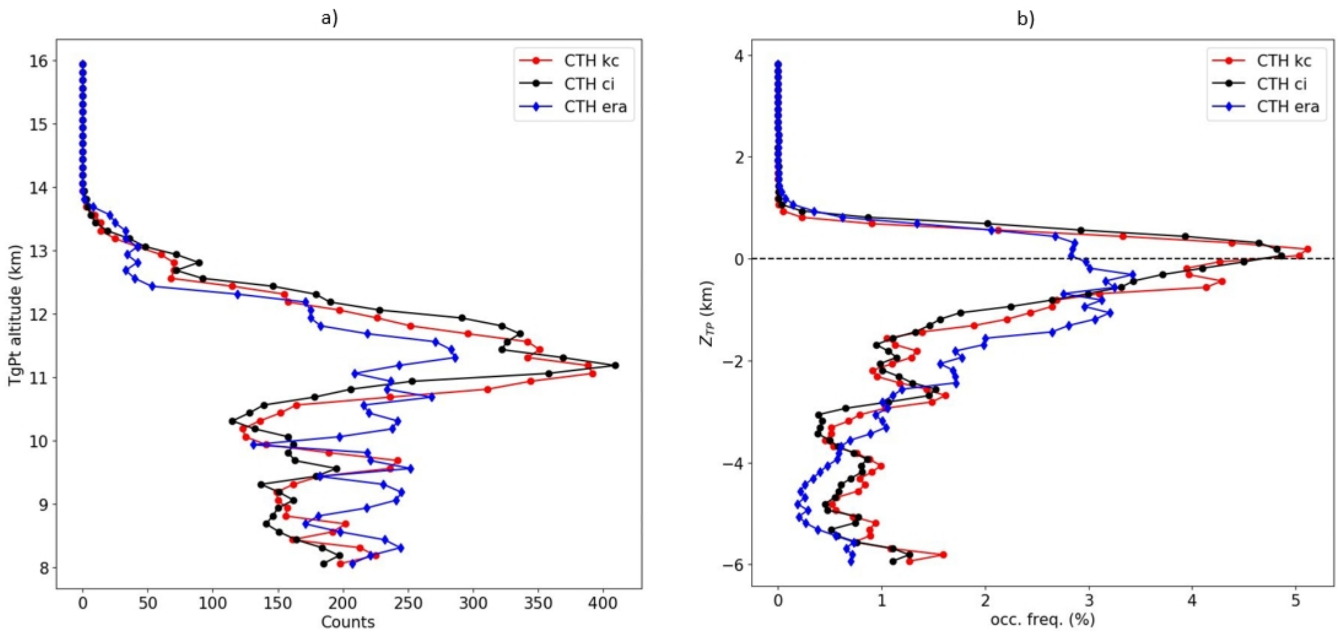

Figure 9. (a) Number of cloud top heights (CTH) per altitude bin for the extinction method (*kc*) in red, the CI method (black) and ERA5 (blue). The altitude of the tangent points (TgPt) is the y axis. (b) The same as a) but using as coordinates the distance of the CTHs to the tropopause in km (Z_{TP}). The used tropopause is the median tropopause (TP_{med}). The three profiles have been were smoothed with a three points running mean.

conservative criterion. This gives confidence to conclude that CTHs above the lapse rate tropopause were detected, even when considering the error in the CTH determination, which is in the order of ± 125 m. Figure 10 shows the distribution of all CTHs and (Fig. 10a) and the distribution of CTHs above TP_{med} (Fig. 10b) for the extinction method. As can be seen, most of the occurrences of CTHs above TP_{med} were found between 50-70° N, with varying altitudes from 8-13 km. The few occurrences between 35-50° N were located at higher altitudes, from 10-14 km. About 6 % of all profiles show for both methods CTHs above the TP_{med} and are classified as optically thin. The ratio of clouds with both CTH and CBH above the TP_{med} is 2 % for the extinction method and 1 % for the CI method. When considering the TP_{95}, both percentages occurrences decrease but still detect CBHs above the TP were detected. The presence of complete layers above the tropopause is inconclusive, as since these CTHs and CBHs are in general just only separated by one altitude bin apart and the CBH is only one or two altitude bins above the tropopause, which is within the uncertainties of the CBH. In Sect. 4.4, a potential case of a cloud layer above the tropopause is discussed in more detail. Our results (summarized in Table 2) agree with previous studies that claim the detection of CTHs above the tropopause for mid-latitudes. Goldfarb et al. (2001) used lidar ground based instruments and found 5 % of CTHs at least 1 km above the tropopause, and approximately 15 % above 0.5 km. Spang et al. (2015) analyzed CRISTA data (Spang et al., 2015) and concluded with a and concluded to a 5 % frequency of occurrence of 5 cirrus clouds (of all observations and Zou et al. (2020) obtained) and Zou et al. (2020) inferred their occurrence to 2 % for CALIPSO data and 4 – 5 % for

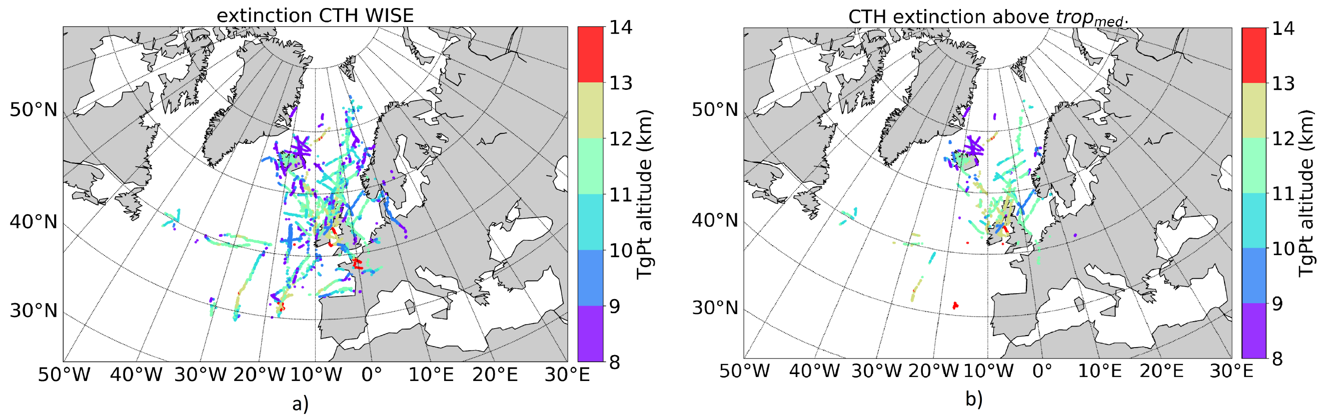

Figure 10. Distribution for (a) all cloud top heights (CTHs) for ~~extinction with color code as~~ the ~~tangent point altitude in km (TgPt)~~ extinction method and (b) CTHs for extinction method above the median tropopause (TP_{med})~~with color code equivalent latitude~~ . Colors indicate the tangent point altitude (~~Eqlat~~TgPt).

MIPAS data. The analyses of Spang et al. (2015) and Zou et al. (2020) used the criterion of the cirrus CTH being 0.5 km above the ~~tropopause derived from~~ ERA-Interim thermal tropopause. Using the same criterion, the frequency of occurrence is 4 % for CTHs above the TP_{med} for the extinction method and 7 % for the CI method. These ~~values~~ occurrence frequencies are comparable to ~~the ones of the literature~~ those reported in the literature (Goldfarb et al., 2001; Spang et al., 2015; Zou et al., 2020). However, as we used ERA5 data, which has a better vertical resolution than ERA-Interim, the equivalent criterion would be to mandate the cirrus CTH to be located 0.25 km above the tropopause. In this case, the frequency of occurrence increases to 13 % above the TP_{med} for the extinction method and to 17 % for the CI method. We explain ~~the~~ these differences in the frequency of occurrence by different periods being compared, the sensitivity and vertical resolution of the instruments, the uncertainty of the meteorological data used to estimate the tropopause height and the definition of stratospheric cirrus used in each study.

4.3 Comparison with ERA5

We compared our CTH detections with the ERA5 ~~data-set~~ dataset by applying the observation geometry of GLORIA. As explained in Sect. 2.3, one of the ~~variables~~ parameters from ERA5 sampled following the viewing geometry of the GLORIA instrument, is the IWC~~for ERA5~~, which when integrated along the LOS results in the limb IWP. Spang et al. (2012) showed that CI and the limb IWP divided by the effective radius of the particles size distribution are very well related to each other. This is ~~caused by the fact that~~ since for large particles (with respect to the wavelength) the observed cloud radiances are determined by the integrated surface area along the LOS, in contrast to the volume density for small particles. We defined a CTH for the ERA5-based ~~data-set~~ dataset to each tangent point with IWP > 0.

Table 2. Percentage with respect to all retrieved profiles Percentages of cloud top heights (CTHs) and cloud bottom heights (CBHs) detected above the median tropopause (TP$_{med}$) and the percentile 95 of the tropopause (TP$_{95}$) relative to all retrieved profiles for both detection methods. The last three rows correspond to the frequency of occurrence of stratospheric cirrus from the studies of Goldfarb et al. (2001), Spang et al. (2015) and Zou et al. (2020).

	TP$_{med}$	TP$_{med}$	TP$_{95}$	TP$_{95}$
	CI	ext	CI	ext
CTH all	27	24	16	13
CTH thin	7	7	5	4
CTH and CBH	1	2	1	1
Goldfarb et al. (2001)	Lidar > 1 km	5		
	Lidar > 0.5 km	15		
Spang et al. (2015)	CRISTA	5		
Zou et al. (2020)	CALIPSO	2		
	MIPAS	4 - 5		

Figure 7c shows a similar distribution of CTHs in pattern of CTHs inferred from ERA5 data as the one those derived from the measurements. The fraction of CTHs detected in ERA5 is about From all investigated profiles, the fraction of detected CTHs is 59 % of all profiles, the same as the one of the CI method (from ERA5, 59 %) and only slightly lower than the fraction for the extinction method (using the CI method and 61 %)the extinction method. Figure 9a shows that between 8 and 11 km altitude, ERA5 indicates more frequent CTHs than the observations. This could be related to not considering discarded multi-layer clouds in the detection algorithm, which would mean could increase the number of CTHs observed between 8 and 11 km, as also CTHs below the first CTH of the multi-layer cloud would be included. The instrument is sensitive to higher and thinner cirrus clouds than the clouds assimilated by ERA5. Consequently, high CTHs detected by GLORIA will hide lower and thicker CTHs in the ERA5-based data-setdataset. When changing to a coordinate system with respect to the TP$_{med}$ (Fig. 9b), the distribution of all CTHs is similar beyond 0.5 km distance from the TP$_{med}$. Between -0.5 km and 0.5 km, there are more CTHs measured than for cirrus measured by GLORIA than present in ERA5. Considering all occurrences When considering all occurrences of cirrus above the TP$_{med}$, the observations detect indicate about 50 % more than cirrus clouds than found in ERA5data-set. This result indicates limitation in the cloud scheme used in the assimilation system of ERA5 for these optically thin clouds close to the tropopause.

4.4 Example of cirrus above the tropopause

In The analysis presented in Sect. 4.2 suggest the presence of complete layers cirrus layers located above the tropopausewas suggested, i.e., both CTH and CBH are were found above the tropopause. As a case study, an observation made during flight 16 on the 21st of October was analyzed in more detail. Figure 11 shows a zoomed area of the cross-section of the flight. Only cloudy points are colored for For both the extinction method and CI. The , measurements with a cloud detection are marked by colors. The altitude for corresponding TP_{med} and TP_{95} have closevaluesare close, indicating that the sampled air masses are were homogeneous with respect to the temperature structure around the tropopause. Both methods identify cirrus cloud at 72.59° N and 69.38° N with CTHs well above the tropopause (∼0.5 to 1 km for the first cirrus cloud and ∼0.5 km for the second). The CBH is slightly higher for the extinction methodand above the tropopauseFor the extinction method, the CBH was located slightly higher than for the CI method, but still within the detection error, therefore, no affirmation of it being undoubtedly . Therefore, the cirrus cannot unambiguously be ascribed to locations above the tropopauseis made. In . At the location of the second cirrus there is was a second tropopause at ∼18 km. Therefore, the CTH of this cirrus is was in between tropopauses. Both clouds are were optically thin, with an extinction between 3×10^{-4} and 5×10^{-3} km^{-1}. The meteorological situation is was characterized by a weak low pressure system on the surface close to Iceland, with an occluded front. The clouds are were located in an area where the wind at 200 hPa changes changed from southwest to west to northwest with velocities between 20 – 28 $km\,h^{-1}$. The air mass in both clouds have had mid-latitude characteristics, with an equivalent latitude of approximately 51° N. The cloud at 72.59° N is was in an area where the PV varies varied from 2.4 to 6 PVU and is was in a stable region with N^2 between 1.6 and 5.2×10^{-4} s^{-2}. These values of Therefore both the PV and N^2 indicate the transition region between troposphere and stratosphere (Kunz et al., 2009, 2011). The cloud at 69.38° N has PV values had a PV characteristic of stratospheric air masses, between 3.7 and 5.7 PVU and large static stability, $5.6 < N^2 < 7.1 \times 10^{-4}$ s^{-2}. Values of N^2 close to 7×10^{-4} s^{-2} are is an indication of mixed sub-tropical and mid-latitudinal air masses (Kunz et al., 2009).

5 Conclusions

In this study, we analyzed cirrus cloud observations taken with the limb sounder GLORIA on board of the research aircraft HALO during the WISE campaign. We used two methods for cloud identification, the cloud index and the derived retrieved extinction coefficient. The analysis focused on high cirrus clouds close to the tropopause and did not include excluded multi-layer clouds. The extinction method indicated very thin clouds with an extinction of as low as 2×10^{-4} km^{-1}. Both methods are in good agreement, having similar frequencies of occurrence and similar CTHs. The main differences are the slightly higher CTHs of the CI method and the higher CBHs from the extinction method. For studying the presence of cloud tops above the tropopause we used two approaches. First, we calculated the median tropopause from ERA5 along the LOS of the GLORIA instrument and second, we used the more conservative 95th percentile. We considered similar tropopauses as an indication of homogeneous air masses. The frequency of occurrence above the tropopause varied from 27 % to 16 % for the CI and from 24 % to 13 % for the extinction method, where the difference between both approaches were due to LOS scenes with heterogeneous tropopause heights. Our results support the higher occurrence frequencies reported in literature (Goldfarb et al., 2001; Spang et al., 2015; Zou et al., 2020) in contrast to lower values frequencies derived from CALIPSO (Pan and Munchak, 2011; Zou et al., 2020) at mid-latitudes. Using the same criterion as in Spang et al. (2015); Zou et al. (2020), i.e. 0.5 km above the tropopause, the frequency of occurrence is 4 % – 7 %. However, as the ERA5 data-set dataset presents a higher vertical resolution, when analyzing the frequency of occurrence 0.250 km above the tropopause, the value fraction increases to 13-17 %. This means, that when the uncertainty of the tropopause estimate and the measurements is smaller, the stratospheric

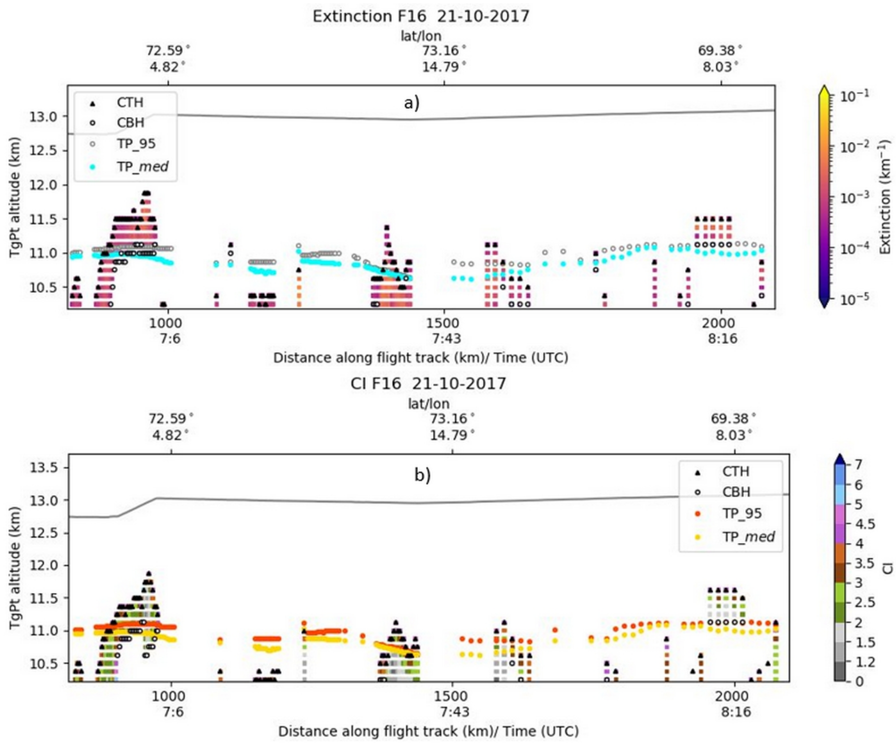

Figure 11. Zoomed area of the cross-section of flight 16 on the 21st of October 2017 focusing on two examples of thin cirrus above the tropopause. (a) Extinction coefficient color scale. Median tropopause (TP_{med}) and the percentile 95 of the tropopause (TP_{95}) are indicated with blue dots and grey dots, respectively. (b) Cloud index color scale. Median tropopause (TP_{med}) and the percentile 95 of the tropopause (TP_{95}) are indicated with yellow dots and orange dots, respectively. Black triangles indicate the CTHs and the white circles the CBHs. The grey line marks the flight trajectory. The altitude of the tangent points (TgPt) is the y axis.

cirrus cloud occurrence frequencies are even higher. 1.5 km below the tropopause both identification methods present good agreement with the clouds indicated by the ERA5 ~~data-set~~dataset, when taken the observation geometry of GLORIA into account. However, the observed occurrence of cloud tops close to and above the tropopause is about 50 % higher than indicated by ERA5. We found CBHs above the tropopause, but they were within the uncertainties. Consequently, the GLORIA WISE campaign data cannot confirm the presence of unattached cirrus layers above the first thermal tropopause, but can confirm the presence of cirrus clouds at the tropopause with CTHs penetrating well into the lower stratosphere.

Data availability. The retrievals can be requested from the author.

Competing interests. The authors declare that they have no conflict of interests.

Acknowledgements. The authors are grateful to the ECMWF for providing operational analysis and forecast as well as reanalysis data. The authors acknowledge funding from the DFG, in the *Cirrus clouds in the extra-tropical tropopause and lowermost stratosphere region (CiTroS) project*, project number SP 969/1-1, part of the HALO Priority Program SPP 1294. Special thanks to the GLORIA team, including the technology institutes ZEA-1 and ZEA-2 at Forschungszentrum Jülich and the Institute for Data Processing and Electronics at the Karlsruhe Institute of Technology. The authors also thank the WISE team, DLR-FX and the pilots.

References

Baran, A. J.: The dependence of cirrus infrared radiative properties on ice crystal geometry and shape of the size-distribution function, Quarterly Journal of the Royal Meteorological Society, 131, 1129–1142, https://doi.org/https://doi.org/10.1256/qj.04.91, 2005.

Blank, J.: Tomographic retrieval of atmospheric trace gases observed by GLORIA, Ph.D thesis, Bergische Universität Wuppertal, Germany, https://juser.fz-juelich.de/record/150342, 2013.

Curtis, A. R.: Discussion of 'A statistical model for water vapour absorption' by R. M. Goody, Quart. J. Roy. Meteorol. Soc., 78, 638–640, 1952.

Davis, S., Hlavka, D., Jensen, E., Rosenlof, K., Yang, Q. O., Schmidt, S., Borrmann, S., Frey, W., Lawson, P., Voemel, H., and Bui, T. P.: In situ and lidar observations of tropopause subvisible cirrus clouds during TC4, J. Geophys. Res., 115, https://doi.org/10.1029/2009JD013093, 2010.

Dessler, A. E.: Clouds and water vapor in the Northern Hemisphere summertime stratosphere, J. Geophys. Res., 114, D00H09, https://doi.org/10.1029/2009JD012075, 2009.

Dudhia, A.: The Reference Forward Model (RFM), J. Quant. Spectrosc. Radiat. Transfer, 186, 243–253, https://doi.org/http://dx.doi.org/10.1016/j.jqsrt.2016.06.018, 2017.

Friedl-Vallon, F., Gulde, T., Hase, F., Kleinert, A., Kulessa, T., Maucher, G., Neubert, T., Olschewski, F., Piesch, C., Preusse, P., Rongen, H., Sartorius, C., Schneider, H., Schoenfeld, A., Tan, V., Bayer, N., Blank, J., Dapp, R., Ebersoldt, A., Fischer, H., Graf, F., Guggenmoser, T., Hoepfner, M., Kaufmann, M., Kretschmer, E., Latzko, T., Nordmeyer, H., Oelhaf, H., Orphal, J., Riese, M., Schardt, G., Schillings, J., Sha, M. K., Suminska-Ebersoldt, O., and Ungermann, J.: Instrument concept of the imaging Fourier transform spectrometer GLORIA, Atmos. Meas. Tech., 7, 3565–3577, https://doi.org/10.5194/amt-7-3565-2014, 2014.

Fusina, F., Spichtinger, P., and Lohmann, U.: Impact of ice supersaturated regions and thin cirrus on radiation in the midlatitudes, J. Geophys. Res., 112, D24S14, https://doi.org/10.1029/2007JD008449, 2007.

Godson, W. L.: The evaluation of infra-red radiative fluxes due to atmospheric water vapour, Quart. J. Roy. Meteorol. Soc., 79, 367–379, 1953.

Goldfarb, L., Keckhut, P., Chanin, M.-L., and Hauchecorne, A.: Cirrus climatological results from lidar measurements at OHP (44°N, 6°E), Geophys. Res. Lett., 28, 1687–1690, https://doi.org/10.1029/2000GL012701, 2001.

Gordley, L. L. and Russell, J. M.: Rapid inversion of limb radiance data using an emissivity growth approximation, Appl. Optics, 20, 807–813, 1981.

Griessbach, S., Hoffmann, L., Hoepfner, M., Riese, M., and Spang, R.: Scattering in infrared radiative transfer: A comparison between the spectrally averaging model JURASSIC and the line-by-line model KOPRA, J. Quant. Spectrosc. Radiat. Transfer, 27, 102–118, https://doi.org/10.1016/j.jqsrt.2013.05.004, 2013.

Griessbach, S., Hoffmann, L., Spang, R., and Riese, M.: Volcanic ash detection with infrared limb sounding: MIPAS observations and radiative transfer simulations, Atmos. Meas. Tech., 7, 1487–1507, https://doi.org/10.5194/amt-7-1487-214, 2014.

Griessbach, S., Hoffmann, L., Spang, R., von Hobe, M., Müller, R., and Riese, M.: Infrared limb emission measurements of aerosol in the troposphere and stratosphere, Atmos. Meas. Tech., 9, 4399–4423, https://doi.org/10.5194/amt-9-4399-2016, 2016.

Griessbach, S., Hoffmann, L., Spang, R., Achtert, P., von Hobe, M., Mateshvili, N., Müller, R., Riese, M., Rolf, C., Seifert, P., and Vernier, J.-P.: Aerosol and cloud top height information of Envisat MIPAS measurements, Atmos. Meas. Tech., 13, 1243–1271, https://doi.org/10.5194/amt-13-1243-2020, 2020.

Hersbach, H., Bell, B., Berrisford, P., Hirahara, S., Horányi, A., Muñoz-Sabater, J., Nicolas, J., Peubey, C., Radu, R., Schepers, D., Simmons, A., Soci, C., Abdalla, S., Abellan, X., Balsamo, G., Bechtold, P., Biavati, G., Bidlot, J., Bonavita, M., De Chiara, G., Dahlgren, P., Dee, D., Diamantakis, M., Dragani, R., Flemming, J., Forbes, R., Fuentes, M., Geer, A., Haimberger, L., Healy, S., Hogan, R. J., Hólm, E., Janisková, M., Keeley, S., Laloyaux, P., Lopez, P., Lupu, C., Radnoti, G., de Rosnay, P., Rozum, I., Vamborg, F., Villaume, S., and Thépaut, J.-N.: The ERA5 global reanalysis, Quart. J. Roy. Meteorol. Soc., 146, 1999–2049, https://doi.org/10.1002/qj.3803, 2020.

Hoffmann, L.: Schnelle Spurengasretrieval für das Satellitenexperiment Envisat MIPAS, Ph.D thesis, Bergische Universität Wuppertal, Germany, ISSN 0944-2952, 2006.

Hoffmann, L., Kaufmann, M., Spang, R., Müller, R., Remedios, J., Moore, D. P., Volk, C. M., von Clarmann, T., and Riese, M.: Envisat MIPAS measurements of CFC-11: retrieval, validation, and climatology, Atmos. Chem. Phys., 8, 3671–3688, 2008.

Höpfner, M. and Emde, C.: Comparison of single and multiple scattering approaches for the simulation of limb-emission observations in the mid-IR, J. Quant. Spectrosc. Radiat. Transfer, 91, 275–285, 2005.

Höpfner, M., Ungermann, J., Borrmann, S., Wagner, R., Spang, R., Riese, M., Stiller, G., Appel, O., Batenburg, A. M., Bucci, S., Cairo, F., Dragoneas, A., Friedl-Vallon, F., Hünig, A., Johansson, S., Krasauskas, L., Legras, B., Leisner, T., Mahnke, C., Möhler, O., Molleker, S., Müller, R., Neubert, T., Orphal, J., Preusse, P., Rex, M., Saathoff, H., Stroh, F., Weigel, R., and Wohltmann, I.: Ammonium nitrate particles formed in upper troposphere from ground ammonia sources during Asian monsoons, Nature Geosciences, 12, 608–612, https://doi.org/10.1038/s41561-019-0385-8, 2019.

IPCC: Climate Change 2013: The Physical Science Basis. Contribution of Working Group I to the Fifth Assessment Report of the Intergovernmental Panel on Climate Change, Cambridge University Press, Cambridge, United Kingdom and New York, NY, USA, https://doi.org/10.1017/CBO9781107415324, 2013.

Kalicinsky, C., Griessbach, S., and Spang, R.: Radiative transfer simulations and observations of infrared spectra in the presence of polar stratospheric clouds: Detection and discrimination of cloud types, Atmos. Meas. Tech. Discuss., 2020, 1–28, https://doi.org/10.5194/amt-2020-144, 2020.

Keckhut, P., Hauchecorne, A., Bekki, S., Colette, A., David, C., and Jumelet, J.: Indications of thin cirrus clouds in the stratosphere at mid-latitudes, Atmos. Chem. Phys., 5, 3407–3414, 2005.

Kent, G. S., Winker, D. M., Vaughan, M. A., Wang, P. H., and Skeens, K. M.: Simulation of Stratospheric Aerosol and Gas Experiment (SAGE) II cloud measurements using airborne lidar data, J. Geophys. Res., 102, 21 795–21 807, https://doi.org/10.1029/97JD01390, 1997.

Kleinert, A., Friedl-Vallon, F., Guggenmoser, T., Höpfner, M., Neubert, T., Ribalda, R., Sha, M., Ungermann, J., Blank, J., Ebersoldt, A., Kretschmer, E., Latzko, T., Oelhaf, H., Olschewski, F., and Preusse, P.: Level 0 to 1 processing of the imaging Fourier transform spectrometer GLORIA: generation of radiometrically and spectrally calibrated spectra, Atmos. Meas. Tech., 7, 4167–4184, https://doi.org/10.5194/amt-7-4167-2014, 2014.

Krämer, M., Rolf, C., Luebke, A., Afchine, A., Spelten, N., Costa, A., Meyer, J., Zoeger, M., Smith, J., Herman, R. L., Buchholz, B., Ebert, V., Baumgardner, D., Borrmann, S., Klingebiel, M., and Avallone, L.: A microphysics guide to cirrus clouds - Part 1: Cirrus types, Atmos. Chem. Phys., 16, 3463–3483, https://doi.org/10.5194/acp-16-3463-2016, 2016.

Krisch, I., Ungermann, J., Preusse, P., Kretschmer, E., and Riese, M.: Limited angle tomography of mesoscale gravity waves by the infrared limb-sounder GLORIA, Atmos. Meas. Tech., 11, 4327–4344, https://doi.org/10.5194/amt-11-4327-2018, 2018.

Kunz, A., Konopka, P., Müller, R., Pan, L., Schiller, C., and Rohrer, F.: High static stability in the mixing layer above the extratropical tropopause, J. Geophys. Res., 114, D16 305, https://doi.org/10.1029/2009JD011840, 2009.

Kunz, A., Konopka, P., Müller, R., and Pan, L. L.: Dynamical tropopause based on isentropic potential vorticity gradients, J. Geophys. Res., 116, D01 110, https://doi.org/10.1029/2010JD014343, 2011.

Liou, K.-N.: Influence of Cirrus Clouds on Weather and Climate Processes: A Global Perspective, Monthly Weather Review, 114, 1167–1199, https://doi.org/10.1175/1520-0493(1986)114<1167:IOCCOW>2.0.CO;2, 1986.

Luebke, A. E., Afchine, A., Costa, A., Grooß, J.-U., Meyer, J., Rolf, C., Spelten, N., Avallone, L. M., Baumgardner, D., and Krämer, M.: The origin of midlatitude ice clouds and the resulting influence on their microphysical properties, Atmos. Chem. Phys., 16, 5793–5809, https://doi.org/10.5194/acp-16-5793-2016, 2016.

Martins, E., Noel, V., and Chepfer, H.: Properties of cirrus and subvisible cirrus from nighttime Cloud-Aerosol Lidar with Orthogonal Polarization (CALIOP), related to atmospheric dynamics and water vapor, Journal of Geophysical Research: Atmospheres, 116, https://doi.org/https://doi.org/10.1029/2010JD014519, 2011.

Noël, V. and Haeffelin, M.: Midlatitude cirrus clouds and multiple tropopauses from a 2002–2006 climatology over the SIRTA observatory, J. Geophys. Res., 112, D13 206, https://doi.org/10.1029/2006JD007753, 2007.

Pan, L. L. and Munchak, L. A.: Relationship of cloud top to the tropopause and jet structure from CALIPSO data, J. Geophys. Res., 116, D12 201, https://doi.org/10.1029/2010JD015462, 2011.

Petty, G. W.: A first Course in Atmospheric Radiation, Sundog Publishing, 2006.

Reverdy, M., Noel, V., Chepfer, H., and Legras, B.: On the origin of subvisible cirrus clouds in the tropical upper troposphere, Atmos. Chem. Phys., 12, 12 081–12 101, https://doi.org/10.5194/acp-12-12081-2012, https://acp.copernicus.org/articles/12/12081/2012/, 2012.

Riese, M., Kaufmann, and M., Hoor, P.: WISE: project description, https://www.halo.dlr.de/science/missions/wise/wise.html, 2017, last accessed: 13 August 2020.

Riese, M., Ploeger, F., Rap, A., Vogel, B., Konopka, P., Dameris, M., and Forster, P.: Impact of uncertainties in atmospheric mixing on simulated UTLS composition and related radiative effects, J. Geophys. Res., 117, D16 305, https://doi.org/10.1029/2012JD017751, 2012.

Riese, M., Oelhaf, H., Preusse, P., Blank, J., Ern, M., Friedl-Vallon, F., Fischer, H., Guggenmoser, T., Hoepfner, M., Hoor, P., Kaufmann, M., Orphal, J., Ploeger, F., Spang, R., Suminska-Ebersoldt, O., Ungermann, J., Vogel, B., and Woiwode, W.: Gimballed Limb Observer for Radiance Imaging of the Atmosphere (GLORIA) scientific objectives, Atmos. Meas. Tech., 7, 1915–1928, https://doi.org/10.5194/amt-7-1915-2014, 2014.

Sassen, K. and Cho, B. S.: Subvisual-thin cirrus lidar data set for satellite verification and climatological research, J. Appl. Met., 31, 1275–1285, 1992.

Sassen, K., Wang, Z., and Liu, D.: Global distribution of cirrus clouds from CloudSat/Cloud-Aerosol Lidar and Infrared Pathfinder Satellite Observations (CALIPSO) measurements, J. Geophys. Res., 113, D00A12, https://doi.org/10.1029/2008JD009972, 2008.

Sembhi, H., Remedios, J., Trent, T., Moore, D. P., Spang, R., Massie, S., and Vernier, J. P.: MIPAS detection of cloud and aerosol particle occurrence in the UTLS with comparison to HIRDLS and CALIOP, Atmos. Meas. Tech., 5, 2537–2553, https://doi.org/10.5194/amt-5-2537-2012, 2012.

Spang, R., Riese, M., and Offermann, D.: CRISTA-2 observations of the south polar vortex in winter 1997: A new dataset for polar process studies, Geophys. Res. Lett., 28, 3159–3162, https://doi.org/10.1029/2000GL012374, 2001.

Spang, R., Hoffmann, L., Kullmann, A., Olschewski, F., Preusse, P., Knieling, P., Schroeder, S., Stroh, F., Weigel, K., and Riese, M.: High resolution limb observations of clouds by the CRISTA-NF experiment during the SCOUT-O3 tropical aircraft campaign, Adv. Space Res., 42, 1765–1775, https://doi.org/10.1016/j.asr.2007.09.036, 2008.

Spang, R., Arndt, K., Dudhia, A., Höpfner, M., Hoffmann, L., Hurley, J., Grainger, R. G., Griessbach, S., Poulsen, C., Remedios, J. J., Riese, M., Sembhi, H., Siddans, R., Waterfall, A., and Zehner, C.: Fast cloud parameter retrievals of MIPAS/Envisat, Atmos. Chem. Phys., 12, 7135–7164, https://doi.org/10.5194/acp-12-7135-2012, 2012.

Spang, R., Günther, G., Riese, M., Hoffmann, L., Müller, R., and Griessbach, S.: Satellite observations of cirrus clouds in the Northern Hemisphere lowermost stratosphere, Atmos. Chem. Phys., 15, 927–950, https://doi.org/10.5194/acp-15-927-2015, 2015.

Spang, R., Hoffmann, L., Höpfner, M., Griessbach, S., Müller, R., Pitts, M. C., Orr, A. M. W., and Riese, M.: A multi-wavelength classification method for polar stratospheric cloud types using infrared limb spectra, Atmos. Meas. Tech., 9, 3619–3639, https://doi.org/10.5194/amt-9-3619-2016, 2016.

Ungermann, J.: On Quantifying and Mitigation GLORIA Instrument Effects and Uncertainties, 2021, in prep.

Ungermann, J., Blank, J., Lotz, J., Leppkes, K., Hoffmann, L., Guggenmoser, T., Kaufmann, M., Preusse, P., Naumann, U., and Riese, M.: A 3-D tomographic retrieval approach with advection compensation for the air-borne limb-imager GLORIA, Atmos. Meas. Tech., 4, 2509 – 2529, https://doi.org/10.5194/amt-4-2509-2011, 2011.

Ungermann, J., Blank, J., Dick, M., Ebersoldt, A., Friedl-Vallon, F., Giez, A., Guggenmoser, T., Höpfner, M., Jurkat, T., Kaufmann, M., Kaufmann, S., Kleinert, A., Krämer, M., Latzko, T., Oelhaf, H., Olchewski, F., Preusse, P., Rolf, C., Schillings, J., and Riese, M.: Level 2 processing for the imaging Fourier transform spectrometer GLORIA: Derivation and validation of temperature and trace gas volume mixing ratios from calibrated dynamics mode spectra, Atmos. Meas. Tech., 8, 2473–2489, https://doi.org/10.5194/amt-8-2473-2015, 2015.

Ungermann, J., Bartolome, I., Grießbach, S., Spang, R., Rolf, C., Krämer, M., Höpfner, M., and Riese, M.: Cirrus cloud shape detection by tomographic extinction retrievals from infrared limb emission sounder measurements, Atmos. Meas. Tech. Discuss., 2020, 1–35, https://doi.org/10.5194/amt-2020-256, 2020.

van de Hulst, H. C.: Light scattering by small particles. By H. C. van de Hulst. New York (John Wiley and Sons), London (Chapman and Hall), 1957. Pp. xiii, 470; 103 Figs.; 46 Tables. 96s, Quarterly Journal of the Royal Meteorological Society, 84, 198–199, https://doi.org/https://doi.org/10.1002/qj.49708436025, 1958.

Wallace, J. and Hobbs, P.: Atmospheric Science: An Introductory Survey, International Geophysics Series, Elsevier Academic Press, 2006.

Weinreb, M. P. and Neuendorffer, A. C.: Method to apply homogeneous-path transmittance models to inhomogenous atmospheres, J. Atmos. Sci., 30, 662–666, 1973.

WMO: Meteorology – A three-dimensional science, WMO Bull, 4, 134–138, 1957.

Yang, P., Gao, B.-C., Baum, B. A., Hu, Y. X., Wiscombe, W. J., Tsay, S.-C., Winker, D. M., and Nasiri, S. L.: Radiative properties of cirrus clouds in the infrared (8–13 μm) spectral region, Journal of Quantitative Spectroscopy and Radiative Transfer, 70, 473 – 504, https://doi.org/https://doi.org/10.1016/S0022-4073(01)00024-3, light Scattering by Non-Spherical Particles, 2001.

Zou, L., Griessbach, S., Hoffmann, L., Gong, B., and Wang, L.: Revisiting global satellite observations of stratospheric cirrus clouds, Atmos. Chem. Phys., 20, 9939–9959, https://doi.org/10.5194/acp-20-9939-2020, 2020.